ARTICLE IN PRESS

Communications Engineering

https://doi.org/10.1038/s44172-026-00597-5

Article in Press

Safe focused ultrasound-mediated blood-brain barrier opening is driven primarily by transient reorganization of tight junctions

Received: 19 May 2025

Accepted: 26 January 2026

Cite this article as: Noel, R.L., Kugelman, T., Karakatsani, M.E. *et al.* Safe focused ultrasound-mediated blood-brain barrier opening is driven primarily by transient reorganization of tight junctions. *Commun Eng* (2026). https://doi.org/10.1038/s44172-026-00597-5

Rebecca Lynn Noel, Tara Kugelman, Maria Eleni Karakatsani, Sanjid Shahriar, Moshe J. Willner, Daniella A. Jimenez, Claire Sunha Choi, Yusuke Nimi, Robin Ji, Dritan Agalliu & Elisa E. Konofagou

We are providing an unedited version of this manuscript to give early access to its findings. Before final publication, the manuscript will undergo further editing. Please note there may be errors present which affect the content, and all legal disclaimers apply.

If this paper is publishing under a Transparent Peer Review model then Peer Review reports will publish with the final article.

ARTICLE IN PRESS

© The Author(s) 2026. **Open Access** This article is licensed under a Creative Commons Attribution-NonCommercial-NoDerivatives 4.0 International License, which permits any non-commercial use, sharing, distribution and reproduction in any medium or format, as long as you give appropriate credit to the original author(s) and the source, provide a link to the Creative Commons licence, and indicate if you modified the licensed material. You do not have permission under this licence to share adapted material derived from this article or parts of it. The images or other third party material in this article are included in the article's Creative Commons licence, unless indicated otherwise in a credit line to the material. If material is not included in the article's Creative Commons licence and your intended use is not permitted by statutory regulation or exceeds the permitted use, you will need to obtain permission directly from the copyright holder. To view a copy of this licence, visit http://creativecommons.org/licenses/by-nc-nd/4.0/.

ARTICLE IN PRESS

Safe focused ultrasound-mediated blood-brain barrier opening is driven primarily by transient reorganization of tight junctions

Rebecca Lynn Noel[1,5], Tara Kugelman[1,5], Maria Eleni Karakatsani[1], Sanjid Shahriar[2], Moshe J. Willner[1], Daniella A. Jimenez[1], Claire Sunha Choi[1], Yusuke Nimi[1], Robin Ji[1], Dritan Agalliu[2,3,6] and Elisa E. Konofagou[1,4,6,7]

1. Department of Biomedical Engineering, Columbia University, 630 W 168th St, New York, 10032, New York, USA.
2. Department of Pathology and Cell Biology, Columbia University, 630 W 168th St, New York, 10032, New York, USA.
3. Department of Neurology, Columbia University, 630 W 168th St, New York, 10032, New York, USA.
4. Department of Radiology, Columbia University Irving Medical Center, New York, NY, 10032, USA.
5. These authors contributed equally to this work.
6. These senior authors equally supervised the work.
7. Corresponding author e-mail: ek2191@columbia.edu

ARTICLE IN PRESS

ARTICLE IN PRESS

Abstract

Focused ultrasound (FUS) with microbubbles opens the blood-brain barrier (BBB) for targeted drug delivery into the brain. How brain endothelial cells (BECs) respond to low acoustic pressures known to open the BBB transiently, or high pressures that cause brain damage, is incompletely characterized. Here, we apply FUS at low (450 kPa) and high (750 kPa) pressures in mice where BBB tight junctions are labelled with eGFP to characterize their abnormalities. Arteriole and capillary BECs respond to low pressure by a transient BBB tight junction reorganization and opening. In contrast, high pressure induces tight junction obliteration and persistent BBB opening in BECs even after 72 hours, associated with microglial activation. Transcriptomic analyses of BECs show that high pressure upregulates genes related to the stress response and cell junction disassembly, whereas low pressure upregulates intracellular repair genes. Thus, transient reorganization and repair of tight junctions mediate safe BBB opening for therapeutic delivery.

Introduction

Targeted delivery of therapeutics to treat neurological and psychiatric diseases remains a challenge due to the presence of the blood-brain barrier (BBB) formed by tight junctions (TJ) between brain endothelial cells (BECs), low rate of caveolar-mediated transport [3–5] and specialized transporters.[1,2] Focused ultrasound (FUS) with systemically delivered microbubbles (<10µm in diameter) is a strategy to increase BBB permeability locally, reversibly and non-invasively to facilitate targeted central nervous system (CNS) drug delivery.[6] At low acoustic pressures, the cavitating microbubbles undergo stable volumetric oscillations (stable cavitation), whereas at high acoustic pressures they undergo inertial cavitation.[7–11] Multiple studies have optimized the frequency,[12] acoustic pressure,[13–15] pulse duration,[16,17] pulse and burst repetition frequency[18] and microbubble size[19,20] for safe BBB opening in rodents, non-human primates[21,22] and humans.[23,24] Using this technology, chemotherapeutic agents,[25–27] antibodies,[28,29] neurotrophic factors,[30,31] adeno-associated viruses,[32,33] and neural stem-cells[34] have been delivered across the BBB.

Although parameters for safe FUS-induced BBB opening (FUS-BBBO) have been worked out, the molecular mechanisms and the transcriptomic response of BECs at low or high acoustic pressures is incompletely characterized. Electron microscopy (EM) studies have shown that FUS with a high acoustic pressure (1MPa), 1.5 MHz or 1.63 MHz center frequency transducer, and 100 ms pulse duration increases caveolae number for transport across the BBB.[35] Similar parameters, but with shorter pulse durations (10 ms), also induces loss of BBB TJ proteins within one hour after FUS by EM.[36] In contrast, pressures ranging from 200 to 800 kPa using a 1.029 MHz and 1.2 MHz center frequency transducer induce a biphasic

ARTICLE IN PRESS

increase in BBB permeability by two-photon imaging, starting with a slow diffusion across larger caliber vessels comparable to transcellular transport, followed by a fast diffusion in smaller caliber vessels comparable to paracellular diffusion.[37,38] Thus, FUS can change both transcellular and paracellular BBB permeability depending on the pressure.

Here, we correlated temporal changes in FUS-BBBO with TJ structural alterations in *eGFP-Claudin5* transgenic mice where TJs are labelled with eGFP[5,39]. We have chosen a 450 kPa (low) pressure associated with safe and reversible BBB opening, and a 750 kPa one (high) known to cause irreversible damage.[40,41] We have selected two time-points: a) 1 hour post-FUS, when the BBB permeability is increased at both pressures, and b) 72 hours post-FUS, when the BBB is resealed at low pressure, but remains open at high pressure.[40,41] We report that FUS-BBBO is associated with permanent damage of BBB TJs in arterioles and capillaries by confocal microscopy within 1 hour at high pressure and these junctions remain unrepaired even at 72 hours. This allows persistent fibrinogen passage and microglial activation. In contrast, at low safe pressures BBB opening and closing is linked to transient TJ reorganizations in arterioles and capillaries in both wild-type (WT) and *Caveolin1 (Cav1)*$^{-/-}$ mice, suggesting a caveolar-independent mechanism. Single-cell RNA sequencing of sorted BECs after FUS-BBBO reveals that transcriptome BEC changes at high pressure at both 1 and 72 hours are dominated by genes related to the "stress response" and "junction protein disassembly", whereas those after lower pressure are driven by "intracellular repair" genes. Thus, low pressures can safely and transiently open the BBB to deliver therapeutics to the brain primarily through transient TJ reorganization.

ARTICLE IN PRESS

Methods

Animals: All experimental procedures involving animals were approved by the Columbia University Institutional Animal Care and Use Committee (IACUC) and in accordance to the Office of Laboratory Animal Welfare and the Association for Assessment and Accreditation of Laboratory Care regulations. A total of eighteen (N=18) male and female C57BL6 or *Tg::eGFP-Claudin5* and three (N=3) male *Tg::eGFP-Claudin5*$^{+/-}$ *Cav1*$^{-/-}$ 12-14 weeks old mice (20-25g) were used for this study. Animals were housed under standard conditions (12 h light/dark cycles, 22°C), were fed a standard rodent chow (3kcal/g; Harlen Laboratories, Indianapolis, IN, USA) and drank distilled water. All mice had access to diet ad libitum. Animals were group housed and were randomly selected into stable (Pressure=0.45MPa) or inertial cavitation (Pressure=0.75MPa) groups.

ARTICLE IN PRESS

Microbubble Preparation: In-house lipid-shelled microbubbles were manufactured as previously published.[61] Briefly, the 1,2-distearoyl-sn-glycero-3-phosphocholine (DSPC) and polyethylene Glycol 2000 (PEG2000) were mixed at a 9:1 ratio. Two milligrams of the mixture was dissolved in a 2-ml solution of filtered PBS/glycerol (10% volume)/propylene glycol (10% volume) with a sonicator (Model 1510, Branson Ultrasonics, Danbury, CT, USA) and stored in a 5 ml vial. The remainder of the vial was filled with decafluorobutane (C_4F_{10}) gas. The vial was then activated via mechanical agitation using VialMix™ shaker (Lantheus Medical Imaging, N. Billerica, MA) for 45 s. The formed microbubbles were analyzed with a Coulter Counter Multisizer (Beckman Coulter Inc., Fullerton, CA).

FUS Blood-Brain Barrier Opening: A single-element 1.5 MHz center frequency focused ultrasound transducer (center frequency: 1.5MHz, focal depth: 60mm, radius: 30mm, axial full width half-maximum intensity: 7.5mm, lateral full-width half-maximum intensity: 1 mm, Imasonic, France) was used for all BBB openings in this study. To measure the beam profile, the transducer was calibrated using a needle hydrophone (HGL-0400, Onda Corp., Sunnyvale, CA) in a tank of deionized, degassed water. The FUS transducer was driven by a function generator (Agilent, Palo Alto, CA, USA) though a 50-dB power amplifier (E&I, Rochester, NY, USA). A pulse-echo transducer (center frequency: 7.5 MHz, focal depth: 60mm, radius 13 mm; Olympus NDT, Waltham, MA) was confocally aligned with the FUS transducer to monitor cavitation events. The pulse-echo transducer was driven by a pulse-receiver (Olympus NDT, Waltham, MA) connected to a digitizer (Gage Applied technologies, Inc., Lachine, QC, Canada) for data acquisition. During passive cavitation detection (PCD) acquisition the pulse-receiver operated in "receive mode" and served as an amplifier during PCD acquisition. The transducer setup was then mounted onto a three-dimensional positioning system (Velmex Inc., Lachine, QC, Canada) for accurate targeting.

A bolus of 1µL/g of body mass of polydisperse microbubbles diluted in ($8X10^8$/mL, mean diameter: 4.5 µm) with 100µL was intravenously injected immediately preceding the sonication. For experiments involving *ex vivo* visualization of biocytin diffusion, mice survived for 1 hr were co-injected with the fluorescent tracer biocytin-tetramethylrhodamine (870 Da, Life Technologies). The caudate putamen is a biologically relevant structure for diseases such as Alzheimer's and Parkinson's, and a structure that has been previously targeted for drug delivery[62]. Targeting of the caudate putamen was achieved by first locating the lambda structure though an intact dilapidated scalp and skull as previously published [63]. Briefly, a water cone filled with deionized (DI), and degassed water was fixed to the FUS transducer, which was submerged in a water bath of DI and degassed water, and finally coupled to the shaved scalp using degassed ultrasound gel. A metallic wire with orthogonal parts was placed above the lambda structure and a C-mode ultrasound was performed to locate the cross and below it, the lambda structure. The FUS transducer was

ARTICLE IN PRESS

then moved via the positioner to the following coordinates from lambda: AP 4.5 mm, ML 2.5 mm and DV -3.5 mm for caudate targeting and a single sonication was performed. The FUS parameters used were as follows: frequency 1.5 MHz, peak-rarefactional pressure 0.45 MPa or 0.75 MPa, pulse length 10 ms, pulse repetition frequency 10 Hz, and for a duration of 120 s.

Magnetic Resonance Imaging: One hour following the ultrasound procedure, all animals underwent scanning with the 9.4T MRI system (Bruker Medical, Boston, MA). The mice were placed in a birdcage coil (diameter 35 mm), while being anesthetized with 1 - 2% isoflurane and respiration rate was monitored throughout the imaging sessions. MR images were acquired using a contrast-enhanced T1-weighted 2D FLASH sequence (TR/TE 230/3.3 ms, flip angle: 70°, number of excitations: 6, field of view: 25.6 mm × 25.6 mm, resolution 100 μm x 100 μm x 400 μm), 45 min following the intraperitoneal bolus injection of 0.3 ml gadodiamide (GD-DTPA) (OmniscanTM, GE Healthcare, Princeton, NJ). As previously reported, gadodiamide provides spatial information of the BBB opening, as it will diffuse into the brain where the BBB disrupted, enhancing MR signal temporarily and enabling *in vivo* visualization of the BBB opening volume.[64] Mice survived for 72 hours, underwent an additional scan of the same sequence, 71 hrs following FUS.

MRI BBB Opening Volume Quantification: Contrast-enhanced T1-weighted MRI images were processed in MATLAB (2019a Mathworks, Natick, MA, USA). Analysis was performed on 15 consecutive coronal images that were manually segmented to remove the skull from the brain. The volume of BBBO, or BBB disruption is defined for the purposes of this study as the volume of the brain into which Gd contrast agent is able to diffuse and be visualized on T1-weighted MRI. This affected volume will be the focus of subsequent histological and transcriptomic analyses. Images were thresholded to generate a binary mask based on the mean plus two standard deviations pixel intensity of an ROI chosen on the contralateral hemisphere. The area of each mask was calculated and summed across all 15 slices to give the final BBB opening volume.

Immunofluorescence Staining and Imaging: For the biocytin-TMR quantification, mice survived for 72 hours, were injected with biocytin-TMR one hour prior to sacrifice. Either 1 or 72 hours post-sonication, mice were transcardially perfused with 30 mL PBS followed by 60 mL 4% paraformaldehyde. The skull was removed and the brain was soaked in paraformaldehyde for six hours, transferred to PBS overnight, cryoprotected in 30% sucrose for 48 hours, and then frozen on dry ice. Brains were coronally sectioned at 25μm throughout the caudate putamen region. A series of 4-6 sections within the focus (1mm) centered at Bregma 0.3 mm were serially selected for each mouse for staining. Tissues were stained for eGFP (1:1000;

ARTICLE IN PRESS

ARTICLE IN PRESS

Sigma-Aldrich, MO), Glut-1 (1:1000; EMD Millipore, MA), DyLight 649 Labeled Griffonia (Bandeiraea) simplicifolia lectin I (1:250; Vector Laboratories, CA), Streptavidin-Alexa594 (1:1000; ThermoFisher) was used to visualize biocytin-TMR distribution in tissues,[39] Iba-1 (1:100; Abcam), CD68 (1:100; Abcam), Fibrinogen (1:500; EMD Millipore, MA), and GFAP (1:1000, Abcam). Whole brain images were captured with an upright Zeiss AxioImager. Confocal images for analysis of tight junction morphology were captured on a Zeiss LSM700 confocal microscope. For each section, 4-6 images were captured on both the contralateral and ipsilateral hemisphere exclusively within the caudate putamen. Images on the ipsilateral hemisphere were acquired near sites of BBB opening, determined by the presence of Biocytin-TMR. Images were minimally processed with Fiji/ImageJ software (NIH) to enhance brightness and contrast.

Flourescent In Situ Hybridization: FISH combined with IF of fresh-frozen sections using antisense mRNA probes for *Egfl7* and *Angpt2* transcripts and Glut-1 (vessel marker) were performed as previously described.[55] The sections were imaged at 20x using a Zeiss LSM900 confocal microscope.

Acoustic Signal Analysis: For each FUS pulse transmitted, microbubble cavitation was acquired by a single element PCD, transferred to a digitizer (GAGE Applied Technologies Inc, Lachine QC, Canada), and processed in MATLAB (2017a Mathworks, Natick, MA, USA). Each PCD pulse was transformed into a power spectrum using a fast Fourier transform (fs= 50 MHz) and the resulting energy spectral density was bandpass filtered (3MHz -9 MHz). The peak value within a 20 kHz bandwidth around each harmonic (nf_c, n=1, 2… 6, f_c=1.5 MHz) and ultraharmonic ($nf_c/2$, n=3, 5, 7, 9) was found. The cavitation dose is computed as the root mean square (rms) of the spectral amplitude for each time point. SCDu and SCDh are given by the CD of their respective bins. The inertial cavitation dose (ICD) is defined as any CD energy not contributing to SCDh or SCDu. The cumulative cavitation dose is given integrating the amplitude over the entire sonication duration. The cumulative cavitation emissions from microbubbles were normalized to baseline cavitation dose measured prior to IV injection of bubbles.

Single-Cell RNA Sequencing Preparation: At either 1 or 72 hours post-FUS, eGFP-Cldn5 mice were deeply anesthetized with 4% isoflurane and perfused for 4 minutes with 4°C, sterile PBS. The brain was dissected into Earl's balanced salt solution (EBSS) and dissociated into a single cell suspension using an established protocol.[55] The single-cell suspension was resuspended in 200 µl of CD16/CD32 Fc block (BD Biosciences, Cat. # 553141; 1/200 in FACS buffer) and incubated at room temperature for 15 minutes. Samples were washed with 2 ml of FACS buffer, and 100 µl were kept aside for unstained and fluorescence minus one (FMO) controls. The samples were washed twice with 2 ml of FACS buffer and resuspended in

ARTICLE IN PRESS

400 µl of propidium iodide (Thermofisher, Cat. # P1304MP; 1/10,000 in FACS buffer). Gates for eGFP fluorescence were set using the wild-type mice lacking eGFP expression in ECs (**Extended Data Figure 8**). The eGFP-Cldn5 positive ECs were sorted out using the BD FACS Aria Flow Cytometer (Columbia Stem Cell Initiative Flow Cytometry Core) and processed for scRNAseq.

Quantification and Statistical Analysis

BBB Leakage and Vessel Size Quantification: Whole brain slices were used to quantify the intensity of the fluorescent tracer Biocytin-TMR and the vasculature by immunofluorescence staining for GLUT-1. Leaky vessels were defined as segmented vessels that colocalized with areas of leakage determined by a fixed threshold. Biocytin-TMR leakage was quantified with a custom algorithm in MATLAB (R2017a, Mathworks, Inc., Natick, MA, USA). For quantification of fluorescence intensity, an ROI of the entire sonicated hemisphere containing the caudate putamen and the other brain structures affected by the FUS focus, such as the somatosensory cortex, was selected for each section in the ipsilateral and contralateral side and fluorescence intensity was calculated by subtracting the selected area times the mean fluorescence of the background from the sum of the pixel values of the ROI. Vessels were identified by GLUT-1 staining, and a custom script written in MATLAB (R2017a, Mathworks, Inc., Natick, MA, USA) segmented vessels and measured the diameter. Leaky vessels were defined as segmented vessels that colocalized with areas of biocytin-TMR leakage determined by a fixed threshold. For quantification of the percentage of leaky vessels for small and large caliber vessels, the number of leaky small, or large, vessels was divided by the total number of small, or large, vessels in the ROI. For each identified vessel the area of biocytin-TMR leakage above a fixed threshold and biocytin-TMR intensity was computed within an ROI centered around the vessel.

TJ Quantification: Maximum intensity projections were created in order to quantify TJ abnormalities. The number of gaps was quantified for each TJ junction strand in leaking vessels on the ipsilateral side, and control vessels on the contralateral side. Vessel boundaries were determined by GLUT-1 staining. Arterioles, venules, and capillaries were identified based on 1) diameter of the vessel to separate capillaries from arteiroles and venules and 2) tight junction structure to distinguish between the three vessel types. Colocalization with leakage of the fluorescent tracer Biocytin-TMR (870 Da) with venules, identified by their TJ morphology, were not found, therefore analysis of venules was excluded from this analysis. Gaps and protrusions are defined as described.[5,39] Only TJ strands contained within vessel boundaries were included in the analysis. Tight junction gap length was measured with Fiji/Image J software (NIH) using maximum intensity projection images from Tg::eGFP-Claudin5 mice one hour after FUS. Histograms of the length of tight junction disruption pooled across mice and vessel type demonstrated a bimodal

ARTICLE IN PRESS

distribution, and a cutoff threshold of 2.5 μm was chosen (**Extended Data Figure 3**). Data was sorted based on gap lengths from 0.4-2.5μm and gaps greater than 2.5 μm.

Immunofluorescence Area Quantification: Maximum intensity projections were created and pixels were thresholded determined by the mean plus two standard deviations of a manually selected ROI containing background noise. For a given immunofluorescent stain, all images underwent the same processing pipeline regardless of hemisphere, pressure, or time point.

Single-Cell RNA Sequencing Analysis: For single-cell RNA sequencing (scRNAseq), the 10x Genomics Chromium platform was used to generate low-depth data (~2000 genes/cell), which was processed using the Cell Ranger analysis pipeline to align reads and generate feature-barcode matrices. The Seurat R package[56] was implemented to read the output of the Cell Ranger pipeline and merge cells from all the samples (untreated controls, high and low FUS pressures, 1 hr. and 72 hr. timepoints) into a single R object. The standard pre-processing workflow for scRNAseq data was carried out in Seurat: cells were filtered based on quality control metrics (number of unique genes detected in each cell > 200, total number of molecules detected within a cell > 1,000 and < 50,000, percentage of reads within a cell that map to the mitochondrial genome < 20, etc.), the data was normalized and scaled, and highly variable features were detected. Next, linear dimensionality reduction (PCA) was performed on the scaled data using the previously determined highly variable features, an alternative heuristic method ('Elbow plot') was implemented to determine the 'dimensionality' of the dataset, and cells were clustered by applying the weighted shared nearest-neighbor graph-based clustering method.[66] Finally, the PCA dimensions were further reduced into two-dimensional space using the non-linear dimensional reduction technique, t-distributed stochastic neighbor embedding (t-SNE), to visualize and explore the scRNAseq dataset and each of its unique clusters. To ensure the purity of endothelial cells in subsequent analysis, all sequenced cells were clustered and the expression levels of canonical cell-type markers Cldn5, Ptprc, Gfap, Pdgfrb, Map2, and Acta2 were evaluated across the clusters. A cluster of contaminating pericytes was identified and excluded based on high expression of Pdgfrb and Acta2. The remaining, pure endothelial cells were then segmented out and clustered again. The expression of vessel subtype markers such as arterial (Bmx, Efnb2, Hey1, and Alpl), capillary (Ivns1abp, Slc1a1, Mfsd2a) and vein (Nr2f2, Len2, and Prcp) were used to identified arterial, capillary and vein endothelial cells as shown in Figure 2C.

Differential Gene Expression Analysis: The Seurat “FindMarkers” function with the default Wilcoxon Rank Sum test was implemented to compile the lists of differentially expressed genes, by comparing

ARTICLE IN PRESS

expression profiles of FUS-BBBO EC clusters to control EC clusters at 450 and 750 kPa, at both acute (1 hr.) and long-term (72 hr.) timepoints.

Gene Set Enrichment Analysis (GSEA): Differential gene expression (DE) analysis was performed to compare gene expression variation between experimental groups[67] and highlight which clusters have further heterogeneity associated with each condition. Following DE analysis, a score was calculated for each gene using the formula: Gene score = -log10(pval) x sign (log2fc). Up- and downregulated genes had a positive and negative score, respectively. The numeric value of the gene score was inversely correlated with the degree of significance, that is, genes that had the highest statistically significant difference in expression and the lowest p-values had the highest score, while non-significant genes with high p-values had a correspondingly low gene score. This score was used to rank each gene in DE gene list. Gene sets relevant to pathways, processes and cell types of interest (blood-brain barrier, VEGF signaling, canonical Wnt/β-catenin signaling, non-canonical Wnt signaling, TGF-β signaling, extracellular matrix, cell-cell adhesion, transporters, Notch signaling, angiogenesis, endothelial cell proliferation, endothelial cell migration, apoptosis, antigen processing and presentation, inflammation, endothelial-to-mesenchymal transition, tip cells) were compiled as part of the overall gene set enrichment analysis, using the GO, KEGG, DAVID and GSEA databases as published previously.[68–70] The ranked list of DE genes, along with the compiled gene sets, were loaded onto GSEA 4.1.0 software, and run through 'GseaPreranked' with the following settings: Number of permutations = 1,000; Collapse/Remap to gene symbols = No_collapse; Max size: exclude larger sets = 1,500; all other settings were left at 'default'. Gene sets with FDR q value ≤ 0.3 were deemed significantly enriched and are included in the GSEA graphs.

Statistical Analysis: Data presented as bar graphs indicate mean ± standard deviation (SD). Dots in bar graph represent individual values per mouse. Pairwise comparisons were calculated with unpaired or paired two-tailed t tests. Comparisons of one or more groups were performed using a 2-way ANOVA and p-values were adjusted based on the Holm Sidak post hoc correction. Statistical analyses were performed in GraphPad Prism (GraphPad Software, San Diego, CA, USA). Statistical details of experiments can be found in figure legends. Sample size was not predetermined using power analysis. Statistical differences between groups in Figure 8 are determined by Wilcoxon rank sum test comparing each group to the untreated control. Significance levels are indicated as follows: *p<0.05; **p<0.01; ***p<0.001; ****p<0.0001.

Results

ARTICLE IN PRESS

FUS increases BBB permeability locally in *eGFP-Claudin5*$^{+/-}$ mice

To analyze temporal changes in FUS-BBBO permeability and TJ morphology by confocal microscopy, we targeted non-invasively a focused ultrasound beam to the left caudate and putamen regions of *eGFP-Claudin5*$^{+/-}$ mice.[5,39] Prior to sonication, mice were injected intravenously with microbubbles and biocytin-TMR, a small (~890 Da) to assess BBB permeability.[5,39,42,43] FUS-BBBO was performed at low[40,44] (450 kPa) and high[40,41] (750 kPa) pressures (**Figure 1A**). Passive cavitation detection signals were collected and cumulative stable and inertial cavitation doses were calculated for each pressure (**Figure 1B**). Harmonic acoustic signals associated with stable cavitation[7] were detected at both pressures and the stable cavitation dose was similar between 450 and 750 kPa (**Extended Data Figure 1)**. At high pressure, ultra-harmonics[45] and broadband emissions were also detected (**Extended Data Figure 1B, D, F**), indicative of inertial cavitation.[7]

BBB leakage was initially assessed with contrast enhanced T1-weighted magnetic resonance imaging (MRI) after injection of Gd-DPTA-BMA (~540 Da) immediately or 71 hours post-FUS. Contrast enhancement (i.e., diffusion of Gd-DPTA-BMA across the BBB) was significantly greater at 1 compared to 72 hours for both pressures, and at 750 kPa compared to 450 kPa by 72 hours (**Figure 1C-E**). Signal enhancement was significantly greater at high compared to low pressure by 72 hours, suggesting restored BBB function at low, but not high, pressure. Similarly, diffusion analysis of biocytin-TMR across the BBB showed a 2- and 3.5-fold higher normalized optical density in the ipsilateral, compared to the contralateral, hemisphere in the striatum/putamen 1 hour after FUS at low and high pressures, respectively (**Figure 1F-H**). The area of biocytin-TMR leakage was 4-fold higher in mice sonicated at 750 kPa compared to 450 kPa 1 hour after FUS (**Figure 1I**). By 72 hours there was no difference between ipsilateral and contralateral hemispheres at 450 kPa, suggesting effective BBB closure (**Figure 1J, L**); however, the biocytin-TMR leakage intensity was 2-fold higher on the ipsilateral hemisphere at 750 kPa, indicating sustained BBB disruption (**Figure 1K, L**). The area of biocytin-TMR leakage at 72 hours after FUS was higher at 750 kPa compared to 450 kPa pressures (**Figure 1M**). These data are consistent with our prior work that BBB opens transiently at low pressures, but remains permeable at higher pressures.

Loss of tight junctions in capillaries and arterioles contributes to persistent FUS-BBBO at high acoustic pressures

To correlate changes in FUS-BBBO at both pressures with TJ structural alterations, we analyzed the number and type of leaky vessels with structural TJ abnormalities in the caudate / putamen via immunofluorescence and confocal imaging at 1 and 72 hours post-FUS. The majority (~90%) of Glut1^{+} leaky vessels had a small

ARTICLE IN PRESS

diameter (<10 µm) for both pressures at 1 hour after FUS (**Figure 2A**). There was a 3-fold increase in the number of small diameter leaky vessels, and a 4-fold increase in the number of large diameter (>10 µm) leaky vessels at high compared to low pressures after 1 hour (**Figure 2A**). A larger percentage of large diameter vessels were leaky at 750 kPa compared to 450 kPa after 1 hour (**Figure 2B**). Thus, higher pressures increase the probability of FUS-BBBO in larger, than smaller, diameter vessels. The larger leaky vessels were exclusively arterioles based on TJ morphology[5,39] and expression of **α**–smooth muscle actin. We could not detect tracer leakage from venules or larger veins. By 72 hours, the average number of leaky vessels at both pressures was lower than 1 hour post-FUS, and most of them were small vessels (**Figure 2C**). However, vessel diameter correlated poorly with the area and intensity of tracer leakage at both pressures and times after FUS-BBBO (**Extended Data Figure 2A-H**). At 72 hours after FUS-BBBO, the percentage of leaky vessels was greater at high compared to low pressure, consistent with persistent biocytin-TMR leakage (**Figure 1J-M**). In contrast, analysis of serum IgG leakage across the BBB was similar between two pressures at 72 hours, likely reflecting an earlier BBB opening (**Extended Data Figure 2I-J**). Therefore, high, but not low, pressure preferentially disrupts larger caliber vessels.

We quantified the fraction of capillary TJs containing gaps larger than 2.5 µm [the cutoff for "pathological gaps" (**Figure 2I**)] in both ipsilateral and contralateral caudate / putamen with confocal microscopy 1 and 72 hours after FUS as described [5,39,43]. There was a 1.5-fold increase in the fraction of TJ strands with large gaps in capillaries for both pressures at 1 hour after FUS, although the lower pressure showed higher variability (**Figure 2E-H", I-J, Extended Data Figure 3**). A large number of leaky capillaries lacking TJ strands were present only at 750 kPa (**Figure 2H', F'**). By 72 hours, there was no difference in the fraction of capillary TJ with large gaps (>2.5 µm) between the ipsilateral and contralateral regions at 450 kPa (**Figure 2K-L", O**), although a significant fraction of capillaries had TJ with large gaps in the ipsilateral hemisphere at 750 kPa (**Figure 2M-N', O**). Thus, high acoustic pressures induce persistent structural damage of capillary TJs by confocal microscopy.

Arterioles constitute a small percentage of leaky vessels at both 1 and 72 hours (**Figure 2A-D**); however, BBB leakage in these vessels has been found in ischemic stroke and TBI leading to persistent brain damage.[121,122] The percentage of TJ strands with large gaps was 4-fold higher in leaky arterioles of the ipsilateral striatum at high pressures 1 hour after FUS-BBBO (**Extended Data Figure 4A-D", I-J**) with no significant difference at low pressure (**Extended Data Figure 4A-B", I-J**). Thus, high pressure induces more acute structural TJ damage in arterioles than capillaries. By 72 hours the fraction of TJs with large gaps was 6-fold higher in the arterioles of the ipsilateral hemisphere with high pressure (**Extended Data Figure 4E-F", I, K**). In contrast, ZO-1 was restored at TJs in Glut1^{+} vessels exposed to both pressures by

ARTICLE IN PRESS

72 hours after FUS (**Extended Data Figure 5**). In summary, at low pressures transient BBB opening correlates with TJ loss and repair, whereas at high pressures there is a persistent structural TJ damage in both capillaries and arterioles that causes long-term BBB opening.

Fibrinogen is a plasma protein involved in coagulation, inflammation and tissue repair that does not normally cross the BBB.[49] Following BBB disruption in neuroinflammation or neurodegeneration, fibrinogen activates microglia triggering neuropathology.[50–54] One hour after the FUS, the area of fibrinogen leakage was higher in the ipsilateral, compared to the contralateral, regions in both pressures (**Extended Data Figure 6A-E**). Fibrinogen leakage was present only near vessels with biocytin-TMR leakage together with ameboid microglia (**Extended Data Figure 6B'', D''**) which were visualized using 3D texture-based volume renderings of 25 µm Z stack confocal images (**Supplementary Movies 1-4**). By 72 hours, we could not detect any fibrinogen at any pressure (**Extended Data Figure 6F-I, J**).

Caveolae-mediated transcellular transport[3–5] is a key component of the BBB, prompting us to evaluate whether upregulation in this process could account for the transient BBB opening at low pressure. We compared BBB permeability after FUS between *eGFP-Claudin5*$^{+/-}$ mice and *eGFP-Claudin5*$^{+/-}$; *Cav1*$^{-/-}$ lacking caveolae. There was no difference in BBB opening volume assessed by MRI, and the area or intensity of biocytin-TMR leakage in the caudate and putamen was similar between two genotypes (**Extended Data Figure 7**). Thus, transient BBB opening at safe pressures is likely not mediated by upregulation in caveolar-mediated transport in BECs.

ARTICLE IN PRESS

Single cell RNA-sequencing of BECs reveals common FUS-induced transcriptome changes within 1 hour regardless of the pressure

To determine the transcriptome response of BECs after FUS-BBBO, we dissociated the caudate / putamen from *eGFP-Claudin5*$^{+/-}$ brains after bilateral FUS into single cells, FACS-sorted eGFP^{+} BECs and performed single-cell RNA sequencing (scRNA-seq) and computational analysis[55] (**Figure 3A, Extended Data Figure 8**, **Supplementary Data 1**). After quality filtering[56] and *in silico* BEC selection based on defined markers [*Pecam1*, *Cldn5*, and *Erg*],[57] we performed graph-based clustering to separate BECs sequenced from 10 brain samples (2 samples per condition and 2 healthy controls; **Supplementary Data 1**) into 20 clusters based on transcriptome expression profiles using high resolution visualized with Uniform Manifold Approximation and Projection (UMAP) (**Figure 3B-D)**. This approach avoids pitfalls arising from incorrect clustering boundaries using lower resolution.[58] We assigned a subtype vessel identity to each BEC cluster based on expression of canonical markers for arteries, capillaries and venules (**Figure 3E, F**). Expression of arterial and venous markers peaked at opposite ends of the UMAP plot separated by capillary

ARTICLE IN PRESS

clusters (**Figure 3E, F**). The second largest variation axis was the FUS-BBBO pressure at 72 hours versus control conditions (healthy BECs). Capillary BECs were the largest population, arterioles BECs comprised the second one, and venule BECs were the smallest population for each condition (**Figure 3G**).

To identify transcriptome signatures differentiating BECs from each condition after FUS-BBBO, we performed differential gene expression (DEG) analysis comparing 1 hour post-FUS (the transcriptome responses of capillary BECs at 450 and 750 kPa were statistically indistinguishable so they were grouped together), 450 kPa 72 hours post-FUS, or 750kPa 72 hours post-FUS to control BEC clusters for each vessel subtype (**Supplementary Data 2-4**). These data were used to conduct gene ontology (GO) analysis in DAVID and gene set enrichment analysis (GSEA) using curated and comprehensive gene catalogs for cellular and molecular pathways and functions from the Molecular Signatures Database v6.1 (*MSigDB: software.broadinstitute.org/ gsea/msigdb/genesets.jsp*),[59,60] and determine which biological processes were significantly up- and downregulated for each condition (**Supplementary Data 5-8**). The transcriptome analysis of capillary BECs one hour-post-FUS revealed upregulation of GO terms related to "cell death (e.g. *Txnip*)", "intracellular signal transduction (e.g. *Hes1, Smad1, Smad6*)," "regulation of cell proliferation (e.g. *Cdhkn1a*)," and "vasculature development (e.g. *Klf4, Hes1*)" relative to untreated controls (**Figure 4A, D; Supplementary Data 2, 5**). Some transcripts related to "vascular development" (*e.g. Pdgfb, Kdr, Lef1, Nrp1*) were downregulated one hour-post-FUS compared to control BECs (**Figure 4A, D, Supplementary Data 2, 5**). These transcriptome BEC changes suggests initiation of a potential repair response in additional to the injury response at the acute phase post-FUS-BBBO.

GSEA analysis of capillary BECs revealed upregulation of "inflammation", "Notch signaling" and "endothelial to mesenchymal transition" 1 hour post-FUS (**Extended Data Figure 9A**). Similar transcriptome changes were seen also in arterioles and venules 1 hour post-FUS. Arterioles exposed to 750 kPa showed increased transcripts related to "regulation of cellular component movement" and "cell-substrate junction", and venules exposed to 450 kPa showed upregulation of "blood vessel development" and "regulation of cellular movement" (**Extended Data Figure 9C, D, Supplementary Data 2, 6, 7**). Therefore, all three BEC subtypes respond dynamically at the acute phase post FUS to upregulate transcripts related to injury (e.g. "cell death", "inflammation") and repair (e.g. "cell proliferation", "cell migration", "vascular development") regardless of the applied pressure.

Distinct FUS-induced transcriptome changes are present in BECs at 72 hours in low versus high pressure

ARTICLE IN PRESS

ARTICLE IN PRESS

The GO term analysis of DEGs upregulated in capillary BECs at 72 hours post – FUS at 450 kPa compared to control BECs revealed upregulation of pathways such as "regulation of cell death" (e.g. *Txnip, Bcl21b*), "intracellular signal transduction," "regulation of cell proliferation" (e.g. *Cdnk1a*), "vascular development" (*Notch1, Notch4, Hes1, Klf4, Clic4*) and "cellular response to stress" (e.g. *Slc2a1, Slc38a2*) (**Figure 4B, D, Supplementary Data 3, 5**). Surprisingly, GSEA analysis of DEGs at 72 hours versus 1 hour post-450 kPa or control BECs showed downregulated pathways for "blood-brain barrier", "cell proliferation", "angiogenesis", "EC migration", "tip cells", "Wnt/β-catenin, Notch and TGF-β signaling" (**Extended Data Figure 9A, B, Supplementary Data 8**). Analysis of key BBB adherens junction (*Cdh5, Ctnna1*) and tight junction (*Cldn5, Ocln, Tjp1, Tjp2, Cngl1*) transcripts revealed that *Cldn5, Cdh5, Tjp1, Cngl1* and *Cnna1* were downregulated more significantly by 1 hour post-FUS at 750 kPa than 450 kPa, and their expression was partially restored by 72 hours at 450 kPa, but not 750 kPa (**Figure 4E-G**). However, *Ocln* and to a certain extent *Tjp1* (ZO-1) was restored by 72 hours at 750 kPa (**Figure 4E-G**). Thus, BECs undergo vascular growth and BBB maturation at 72 hours post-FUS at both pressures.

Similarly, the GO term analysis of DEGs upregulated in capillary BECs at 72 hours post- FUS at 750 kPa showed also upregulation of pathways related to "cell death" (e.g. *Txnip, Bcl21b*), "intracellular signal transduction," "regulation of cell proliferation" (e.g. *Cdnk1a*), and "vascular development" (*e.g. Notch1, Notch4, Hes1, Klf4, Clic4*) compared to control ECs (**Figure 4B, D**). In contrast to 450 kPa, GSEA analysis revealed that processes such as "blood-brain barrier", "inflammation", "tip cells" were upregulated at 72 hour post-750 kPa, whereas "angiogenesis", "EC migration", "VEGF", "TGF-β" and "non-canonical Wnt signaling" were downregulated compared to controls (**Extended Data Figure 9A, B, Supplementary Data 8**). Pathway analysis of upregulated DEGs in ECs after 72 hours after 750 kPa compared to 450 kPa revealed upregulation of "protein complex assembly," (e.g. *Arpc1b, Arpc3, Actr3, Atp5d, Atp5g1*), "cell death," and "wound response" (e.g. *CD81, CD151, Ppia*) (**Figure 4C, D**). These transcriptome findings are consistent with the structural TJ analysis that BECs exposed to 450 kPa mostly recover by 72 hours post-FUS, whereas those exposed to 750 kPa are still undergoing cell death and repair due to severe damage.

Signaling pathways related to angiogenesis and barriergenesis change dynamically in BECs after FUS-BBBO

In order to understand which signaling pathways critical for angiogenesis and barriergenesis change in BECs after FUS, we performed a GSEA analysis. TGF-β signaling, which inhibits cell proliferation, suppresses inflammation and promotes vascular development, is upregulated in capillary BECs 1 hour post-FUS consistent with increased inflammatory response (**Figure 5A; Supplementary Data 5, 8).** However, Several TGF-β signaling genes (e.g. *Tgfb2*, Tgfbr2) were significantly downregulated in BECs exposed to

ARTICLE IN PRESS

750 kPa at 72 hours post-FUS relative to other conditions (**Figure 5A; Supplementary Data 5, 8**), consistent with onset of angiogenesis.

Notch signaling, which is an important regulator of angiogenesis and BEC proliferation, changed dynamically after FUS. Notch signaling components (*e.g. Rbpj, Adam100)* were upregulated significantly in capillary BECs one hour post-FUS compared to control (**Figures 5A; Supplementary Data 5, 8**). However, the Notch pathway was largely downregulated by 72 hours post-FUS in capillary and arteriole BECs, relative to other conditions (**Figures 5D; Supplementary Data 5, 8**). In addition, arteriole BECs showed decreased VEGF signaling at 72 hours post 750 kPa relative to untreated controls (**Figure 5A**). When comparing arterioles exposed to 750 kPa to those exposed to 450 kPa 72 hours post-FUS, GSEA analysis reveals increased expression of TGF-β and VEGF signaling. Overall, pathways critical for angiogenesis and BEC proliferation change dynamically after FUS-BBBO.

Wnt/β-catenin signaling is critical for CNS angiogenesis and BBB maturation, prompting us to examine its transcriptome changes after FUS-BBBO. GO and GSEA analyses did not show any significant changes in Wnt/β-catenin signaling in either pressure at the acute phase, however, this pathway was decreased at both pressures at 72 hours compared to 1 hour post-FUS (**Figure 5A, Supplementary Data 5, 8**). Additionally, arterioles exposed to both pressures showed decreased expression of Wnt/β-catenin signaling at 72 compared to 1 hour post-FUS (**Supplementary Data 6**). Overall, this analysis indicates a "return to normalization" at both pressures by 72 hours post-FUS, since Wnt/β-catenin signaling is reduced once angiogenesis and BBB maturation are complete.[1,2]

We validated some of the scRNA-seq findings related to "angiogenesis" using fluorescent in situ hybridization (FISH) for two angiogenesis markers *Egfl7* and *Angpt2* [55] combined with a vessel marker (Glut-1, **Figures 6, Extended Data Figure 10**). Violin plots from scRNA-seq data revealed significant increase for *Egfl7* and *Angpt2* mRNAs in the pooled 1 hour pressure group, and at 72 hours in both 450 and 750 kPa relative to untreated controls by Wilcoxon rank sum test (**Figures 6A, Extended Data Figure 10A**). By FISH, *Egfl7* mRNA was slightly upregulated in Glut1^{+} vessels exposed to 450 kPa on the ipsilateral hemispheres, whereas we could not detect any *Angpt2* mRNA (**Figure 6B, C** and **Extended Data Figure 10B, C**). In contrast both *Egfl7* and *Angpt2* mRNAs were highly upregulated in Glut-1^{+} vessels exposed to 750 kPa on the ipsilateral hemisphere (**Figure 6D, E** and **Extended Data Figure 10D, E**). These findings validate the scRNA-seq data that "angiogenesis" is upregulated at 72 hours in both pressures, with a more sustained response in the high pressure. Thus, FUS-BBBO promotes an "angiogenic" program in CNS blood vessels to drive vascular repair in particular at high pressure.

ARTICLE IN PRESS

Discussion

FUS with microbubbles allows non-invasive, localized, and transient BBB opening to deliver drugs into the brain. However, the cell biological mechanisms and transcriptome changes by which BECs respond to FUS-BBBO are not fully characterized. Here we show that BBB TJ structural integrity is compromised for a longer period (72 hours) at high, but not low, pressures in capillaries and to a lesser extent in arterioles. The diameter of cavitating microbubbles matches more closely to capillaries than arterioles, allowing a higher probability of physical interactions with the vessel wall.[72] This may explain why the microbubbles are more efficient to disrupt capillaries TJs at both pressures. With increasing vessel diameter, there is increased microbubble expansion[73,74] and inertial cavitation threshold,[75] due to changes in the resonance frequency of the bubbles, or additional constraints in the microvasculature.[76,77] Therefore, microstreaming and shock waves may occur more often in larger vessels,[7–11] which is supported by our findings that higher pressure disrupts TJs in larger caliber vessels. Although we could not detect any damaged venules at either pressure, structural BBB changes have been reported in venules by EM at very high pressures (1 MPa), albeit less frequent than capillaries and arterioles.[78] Future EM studies will provide higher resolution related to vessel selectivity in BBB opening with low safe pressures.

BBB TJs undergo remodeling in neurological diseases.[5,39,79,80] Under stable cavitation, we find significant abnormalities in both capillary and arteriole TJs with gaps within 1 hour post FUS at both pressures that likely underlie FUS-BBBO. However, by 72 hours, there is no difference in the fraction of TJ segments with larger gaps (>2.5 μm) between the two hemispheres for 450 kPa, consistent with transient BBB opening. TJ protein degradation may occur as quickly as 20 minutes following sonication[38] and TJ strands may start repairing within 1 hour post FUS-BBBO at low pressure. Our transcriptome analysis of BECs within 1 hour post FUS revealed that "cellular responses to stress" and "junctional protein synthesis" are upregulated to cope with injury; however, this response resolves to baseline by 72 hours post-FUS. Stable cavitation may change the turnover of TJ membrane proteins or stability of ZO proteins that anchor TJ transmembrane proteins to the cytoskeleton.[81] Under high pressure, capillaries exhibited a full absence of TJ strands, a phenomenon likely induced by shock waves generated by microbubble collapse. These TJ abnormalities are not repaired by 72 hours suggesting a permanent BBB TJ damage. Transcriptome analysis of BECs exposed to 750 kPa confirmed the presence of cell biological processes that sustained injury (e.g. "cell death") and repair processes (e.g. "cell proliferation", "cell migration", "vascular development") at both acute and long-term timepoints at 750 kPa. Removal of complete TJ segments may not permit BECs to restore cell-cell junctions by 72 hours, albeit this process begins, leading to longer-term BBB impairment.

ARTICLE IN PRESS

ARTICLE IN PRESS

Although transient opening of the BBB at low pressure may be promoted by caveolae, our findings do not support this hypothesis as there is no differences in BBB opening between wild-type and *Cav1*$^{-/-}$ mice at 450 kPa. Increased number of caveolae have been reported in arterioles using lower center frequency transducer after FUS-BBBO[78,82,83] and caveolae-mediated endocytosis may be important for transporting large molecules across the BBB.[84] Future transcriptomic analysis of *Cav1*$^{-/-}$ BECs after FUS-BBBO will address this question in more depth.

The transcriptome analysis of BECs after FUS-BBBO revealed that arterioles, capillary and venules respond uniformly at the acute phase (1 hour) to upregulate transcripts related to injury (e.g. "cell death", "inflammation") and repair (e.g. "cell proliferation", "cell migration", "vascular development") regardless of the pressure. In contrast, there are distinct transcriptome BEC responses between the two pressures by 72 hours post-FUS. Capillary BECs upregulate pathways related to "cell death", "signal transduction," "cell proliferation", "vascular development" and "cellular response to stress" by 72 hours at both pressures. Surprisingly, GSEA analysis showed downregulated pathways for "blood-brain barrier", "cell proliferation", "angiogenesis", "EC migration", "tip cells", "Wnt/β-catenin, Notch and TGFβ signaling" in BECs from 450 kPa by 72 hours indicative of an ongoing repair. GSEA analysis revealed that processes such as "blood-brain barrier", "inflammation", "tip cells" were upregulated at 72 hour post-FUS at 750 kPa, whereas those related to "angiogenesis", "EC migration", "VEGF, TGFβ and non-canonical Wnt signaling" were downregulated compared to controls. Moreover, transcriptome comparison of BECs from 750 kPa and 450 kPa revealed the presence of pathways related to "protein complex assembly," "cell death," and "wound response". In summary, BECs from 450 kPa are likely still undergoing vascular growth and BBB maturation at 72 hours post-FUS. Our transcriptome findings are consistent with the idea that BECs exposed to low safe pressure recover by 72 hours post-FUS, whereas those exposed to high damaging pressures are still undergoing cell death and repair.

Two angiogenesis promoting pathways, TGF-β and Notch signaling, change dynamically after FUS-BBBO. TGF-β signaling which inhibits cell proliferation, suppresses inflammation and promotes vascular development, is upregulated in capillary BECs one hour post-FUS together with inflammatory responses. However, it is largely downregulated by 72 hours relative to control BECs, consistent with reduced inflammation and induction of angiogenesis. Notch signaling is also upregulated significantly in capillary BECs one hour post-FUS; however, it is shut down by 72 hours post-FUS in capillary BECs, in particular for 750 kPa. Therefore, several signaling pathways critical for angiogenesis and BEC proliferation change dynamically after FUS, but they remain lower in high pressure condition by 72 hours consistent with more

ARTICLE IN PRESS

vessel damage. Although, Wnt/β-catenin signaling was not changed at the acute phase for both pressures, it was reduced at both pressures by 72 hours indicative of a "return to normalization" since this pathway is reduced once angiogenesis and BBB maturation are complete.[1,2]

Clinical trials employ lower frequencies compared to 1.5 MHz used in this study to reduce aberrations caused by the skull and increase the focal volume. While well-suited for human studies, lower frequencies pose challenges in small animal studies including the formation of standing waves creating peaks of high pressure associated with damage and heating.[117–119] Microbubble diameter and the resonance frequency of the transducer will affect how microbubbles oscillate within the vasculature.[19,74] As clinical trials utilizing FUS-BBBO for tumor therapy are under way,[23,120] a rigorous understanding of neurovascular recovery including other cell types will further aid in harnessing this technique for therapeutic treatment.

Data Availability

The raw and analyzed mouse BEC scRNA-seq datasets supporting this manuscript are archived at the NIH GEO repository under accession number GSE253425. The source data files for the Main and Extended Data figures associated with this manuscript can be provided to the readers upon request.

Code Availability

No commercial code was used in the manuscript. We can provide the code used in R for the analysis of single cell RNA sequencing data to the readers upon request.

ARTICLE IN PRESS

References

1. Liebner, S. *et al.* Functional morphology of the blood-brain barrier in health and disease. *Acta Neuropathol. (Berl.)* **135**, 311–336 (2018).
2. Biswas, S., Cottarelli, A. & Agalliu, D. Neuronal and glial regulation of CNS angiogenesis and barriergenesis. *Dev. Camb. Engl.* **147**, dev182279 (2020).
3. Ben-Zvi, A. *et al.* Mfsd2a is critical for the formation and function of the blood-brain barrier. *Nature* **509**, 507–511 (2014).
4. Andreone, B. J. *et al.* Blood-Brain Barrier Permeability Is Regulated by Lipid Transport-Dependent Suppression of Caveolae-Mediated Transcytosis. *Neuron* **94**, 581-594.e5 (2017).
5. Lutz, S. E. *et al.* Caveolin1 Is Required for Th1 Cell Infiltration, but Not Tight Junction Remodeling, at the Blood-Brain Barrier in Autoimmune Neuroinflammation. *Cell Rep.* **21**, 2104–2117 (2017).

ARTICLE IN PRESS

6. Meng, Y. *et al.* Safety and efficacy of focused ultrasound induced blood-brain barrier opening, an integrative review of animal and human studies. *J. Controlled Release* **309**, 25–36 (2019).
7. Leighton, T. G. *The Acoustic Bubble*. (Academic Press, 1997).
8. Miller, D. L. Particle gathering and microstreaming near ultrasonically activated gas-filled micropores. *Cit. J. Acoust. Soc. Am.* **84**, 1378 (1988).
9. Kodama, T. & Tomita, Y. Cavitation bubble behavior and bubble-shock wave interaction near a gelatin surface as a study of in vivo bubble dynamics. *Appl. Phys. B Lasers Opt.* **70**, 139–149 (2000).
10. Prentice, P., Cuschieri, A., Dholakia, K., Prausnitz, M. & Campbell, P. Membrane disruption by optically controlled microbubble cavitation. *Nat. Phys.* **1**, 107–110 (2005).
11. Qin, S. & Ferrara, K. W. Acoustic response of compliable microvessels containing ultrasound contrast agents. *Phys. Med. Biol.* **51**, 5065–88 (2006).
12. McDannold, N., Vykhodtseva, N. & Hynynen, K. Blood-brain barrier disruption induced by focused ultrasound and circulating preformed microbubbles appears to be characterized by the mechanical index. *Ultrasound Med. Biol.* **34**, 834–40 (2008).
13. Vlachos, F., Tung, Y.-S. & Konofagou, E. Permeability dependence study of the focused ultrasound-induced blood-brain barrier opening at distinct pressures and microbubble diameters using DCE-MRI. *Magn. Reson. Med.* **66**, 821–830 (2011).
14. Samiotaki, G., Vlachos, F., Tung, Y.-S. & Konofagou, E. E. A quantitative pressure and microbubble-size dependence study of focused ultrasound-induced blood-brain barrier opening reversibility in vivo using MRI. *Magn. Reson. Med.* **67**, 769–777 (2012).
15. O'Reilly, M. A., Hough, O. & Hynynen, K. Blood-Brain Barrier Closure Time After Controlled Ultrasound-Induced Opening Is Independent of Opening Volume. *J. Ultrasound Med. Off. J. Am. Inst. Ultrasound Med.* **36**, 475–483 (2017).
16. Samiotaki, G. & Konofagou, E. E. Dependence of the reversibility of focused- ultrasound-induced blood-brain barrier opening on pressure and pulse length in vivo. *IEEE Trans. Ultrason. Ferroelectr. Freq. Control* **60**, 2257–2265 (2013).
17. O'Reilly, M. A., Waspe, A. C., Ganguly, M. & Hynynen, K. Focused-ultrasound disruption of the blood-brain barrier using closely-timed short pulses: influence of sonication parameters and injection rate. *Ultrasound Med. Biol.* **37**, 587–94 (2011).
18. Choi, J. J. *et al.* Noninvasive and localized blood-brain barrier disruption using focused ultrasound can be achieved at short pulse lengths and low pulse repetition frequencies. *J. Cereb. Blood Flow Metab. Off. J. Int. Soc. Cereb. Blood Flow Metab.* **31**, 725–37 (2011).
19. Choi, J. J. *et al.* Microbubble-Size Dependence of Focused Ultrasound-Induced Blood–Brain Barrier Opening in Mice *In Vivo*. *IEEE Trans. Biomed. Eng.* **57**, 145–154 (2010).

ARTICLE IN PRESS

ARTICLE IN PRESS

20. McMahon, D. & Hynynen, K. Acute Inflammatory Response Following Increased Blood-Brain Barrier Permeability Induced by Focused Ultrasound is Dependent on Microbubble Dose. *Theranostics* **7**, 3989–4000 (2017).
21. Marquet, F., Tung, Y.-S., Teichert, T., Ferrera, V. P. & Konofagou, E. E. Noninvasive, Transient and Selective Blood-Brain Barrier Opening in Non-Human Primates In Vivo. *PLoS ONE* **6**, e22598 (2011).
22. McDannold, N., Arvanitis, C. D., Vykhodtseva, N. & Livingstone, M. S. Temporary disruption of the blood-brain barrier by use of ultrasound and microbubbles: safety and efficacy evaluation in rhesus macaques. *Cancer Res.* **72**, 3652 (2012).
23. Mainprize, T. *et al.* Blood-Brain Barrier Opening in Primary Brain Tumors with Non-invasive MR-Guided Focused Ultrasound: A Clinical Safety and Feasibility Study. *Sci. Rep.* **9**, 321 (2019).
24. Lipsman, N. *et al.* Blood–brain barrier opening in Alzheimer's disease using MR-guided focused ultrasound. *Nat. Commun.* **9**, 2336 (2018).
25. Treat, L. H. *et al.* Targeted delivery of doxorubicin to the rat brain at therapeutic levels using MRI-guided focused ultrasound. *Int. J. Cancer* **121**, 901–907 (2007).
26. Park, E.-J., Zhang, Y.-Z., Vykhodtseva, N. & McDannold, N. Ultrasound-mediated blood-brain/blood-tumor barrier disruption improves outcomes with trastuzumab in a breast cancer brain metastasis model. *J. Controlled Release* **163**, 277–284 (2012).
27. Kinoshita, M., McDannold, N., Jolesz, F. A. & Hynynen, K. Noninvasive localized delivery of Herceptin to the mouse brain by MRI-guided focused ultrasound-induced blood-brain barrier disruption. *Proc. Natl. Acad. Sci.* **103**, 11719–11723 (2006).
28. Jordão, J. F. *et al.* Antibodies Targeted to the Brain with Image-Guided Focused Ultrasound Reduces Amyloid-β Plaque Load in the TgCRND8 Mouse Model of Alzheimer's Disease. *PLoS ONE* **5**, e10549 (2010).
29. Kinoshita, M., McDannold, N., Jolesz, F. A. & Hynynen, K. Targeted delivery of antibodies through the blood–brain barrier by MRI-guided focused ultrasound. *Biochem. Biophys. Res. Commun.* **340**, 1085–1090 (2006).
30. Samiotaki, G., Acosta, C., Wang, S. & Konofagou, E. E. Enhanced Delivery and Bioactivity of the Neurturin Neurotrophic Factor through Focused Ultrasound—Mediated Blood—Brain Barrier Opening *in vivo*. *J. Cereb. Blood Flow Metab.* **35**, 611–622 (2015).
31. Baseri, B. *et al.* Activation of signaling pathways following localized delivery of systemically administered neurotrophic factors across the blood–brain barrier using focused ultrasound and microbubbles. *Phys. Med. Biol.* **57**, N65–N81 (2012).

ARTICLE IN PRESS

ARTICLE IN PRESS

32. Wang, S., Olumolade, O. O., Sun, T., Samiotaki, G. & Konofagou, E. E. Noninvasive, neuron-specific gene therapy can be facilitated by focused ultrasound and recombinant adeno-associated virus. *Gene Ther.* **22**, 104–110 (2015).
33. Thévenot, E. *et al.* Targeted Delivery of Self-Complementary Adeno-Associated Virus Serotype 9 to the Brain, Using Magnetic Resonance Imaging-Guided Focused Ultrasound. *Hum. Gene Ther.* **23**, 1144–1155 (2012).
34. Burgess, A. *et al.* Targeted delivery of neural stem cells to the brain using MRI-guided focused ultrasound to disrupt the blood-brain barrier. *PloS One* **6**, e27877 (2011).
35. Sheikov, N., McDannold, N., Vykhodtseva, N., Jolesz, F. & Hynynen, K. Cellular mechanisms of the blood-brain barrier opening induced by ultrasound in presence of microbubbles. *Ultrasound Med. Biol.* **30**, 979–989 (2004).
36. Sheikov, N., McDannold, N., Sharma, S. & Hynynen, K. Effect of focused ultrasound applied with an ultrasound contrast agent on the tight junctional integrity of the brain microvascular endothelium. *Ultrasound Med. Biol.* **34**, 1093–104 (2008).
37. Raymond, S. B., Skoch, J., Hynynen, K. & Bacskai, B. J. Multiphoton Imaging of Ultrasound/Optison Mediated Cerebrovascular Effects *in vivo*. *J. Cereb. Blood Flow Metab.* **27**, 393–403 (2007).
38. Nhan, T. *et al.* Drug delivery to the brain by focused ultrasound induced blood-brain barrier disruption: quantitative evaluation of enhanced permeability of cerebral vasculature using two-photon microscopy. *J. Control. Release Off. J. Control. Release Soc.* **172**, 274–280 (2013).
39. Knowland, D. *et al.* Stepwise recruitment of transcellular and paracellular pathways underlies blood-brain barrier breakdown in stroke. *Neuron* **82**, 603–17 (2014).
40. Sun, T. *et al.* Acoustic cavitation-based monitoring of the reversibility and permeability of ultrasound-induced blood-brain barrier opening. *Phys. Med. Biol.* **60**, 9079–94 (2015).
41. Tung, Y.-S., Marquet, F., Teichert, T., Ferrera, V. & Konofagou, E. E. Feasibility of noninvasive cavitation-guided blood-brain barrier opening using focused ultrasound and microbubbles in nonhuman primates. *Appl. Phys. Lett.* **98**, 163704 (2011).
42. Lengfeld, J. E. *et al.* Endothelial Wnt/β-catenin signaling reduces immune cell infiltration in multiple sclerosis. *Proc. Natl. Acad. Sci.* **114**, E1168–E1177 (2017).
43. Platt, M. P. *et al.* Th17 lymphocytes drive vascular and neuronal deficits in a mouse model of postinfectious autoimmune encephalitis. *Proc. Natl. Acad. Sci. U. S. A.* **117**, 6708–6716 (2020).
44. Karakatsani, M. E. *et al.* Amelioration of the nigrostriatal pathway facilitated by ultrasound-mediated neurotrophic delivery in early Parkinson's disease. *J. Controlled Release* **303**, 289–301 (2019).
45. Prosperetti, A. A general derivation of the subharmonic threshold for non-linear bubble oscillations. *J. Acoust. Soc. Am.* **133**, 3719–3726 (2013).

ARTICLE IN PRESS

ARTICLE IN PRESS

46. Davalos, D. *et al.* ATP mediates rapid microglial response to local brain injury in vivo. *Nat. Neurosci.* **8**, 752–758 (2005).
47. Lou, N. *et al.* Purinergic receptor P2RY12-dependent microglial closure of the injured blood-brain barrier. *Proc. Natl. Acad. Sci. U. S. A.* **113**, 1074–9 (2016).
48. Roth, T. L. *et al.* Transcranial amelioration of inflammation and cell death after brain injury. *Nature* **505**, 223–8 (2014).
49. Davalos, D. & Akassoglou, K. Fibrinogen as a key regulator of inflammation in disease. *Semin. Immunopathol.* **34**, 43–62 (2012).
50. Davalos, D. *et al.* Fibrinogen-induced perivascular microglial clustering is required for the development of axonal damage in neuroinflammation. *Nat. Commun.* **3**, 1227 (2012).
51. Adams, R. A. *et al.* The fibrin-derived γ377-395 peptide inhibits microglia activation and suppresses relapsing paralysis in central nervous system autoimmune disease. *J. Exp. Med.* **204**, 571–582 (2007).
52. Cortes-Canteli, M. *et al.* Fibrinogen and β-Amyloid Association Alters Thrombosis and Fibrinolysis: A Possible Contributing Factor to Alzheimer's Disease. *Neuron* **66**, 695–709 (2010).
53. Petersen, M. A., Ryu, J. K. & Akassoglou, K. Fibrinogen in neurological diseases: mechanisms, imaging and therapeutics. *Nat. Rev. Neurosci.* **19**, 283–301 (2018).
54. Ryu, J. K. *et al.* Blood coagulation protein fibrinogen promotes autoimmunity and demyelination via chemokine release and antigen presentation. *Nat. Commun.* **6**, (2015).
55. Shahriar, S. *et al.* Single-cell RNA-sequencing implicates venous endothelial cells as a source of VEGF-A-mediated neo-angiogenesis in neuroinflammation. Preprint at https://doi.org/10.1101/2022.11.15.516660 (2022).
56. Hao, Y. *et al.* Integrated analysis of multimodal single-cell data. *Cell* **184**, 3573-3587.e29 (2021).
57. Vanlandewijck, M. *et al.* A molecular atlas of cell types and zonation in the brain vasculature. *Nature* **554**, 475–480 (2018).
58. Miao, Z. *et al.* Putative cell type discovery from single-cell gene expression data. *Nat. Methods* **17**, 621–628 (2020).
59. Zarkada, G. *et al.* Specialized endothelial tip cells guide neuroretina vascularization and blood-retina-barrier formation. *Dev. Cell* **56**, 2237-2251.e6 (2021).
60. Zhao, Q. *et al.* Single-Cell Transcriptome Analyses Reveal Endothelial Cell Heterogeneity in Tumors and Changes following Antiangiogenic Treatment. *Cancer Res.* **78**, 2370–2382 (2018).
61. Wang, S., Samiotaki, G., Olumolade, O., Feshitan, J. A. & Konofagou, E. E. Microbubble type and distribution dependence of focused ultrasound-induced blood-brain barrier opening. *Ultrasound Med. Biol.* **40**, 130–137 (2014).

ARTICLE IN PRESS

ARTICLE IN PRESS

62. Samiotaki, G., Acosta, C., Wang, S. & Konofagou, E. E. Enhanced delivery and bioactivity of the neurturin neurotrophic factor through focused ultrasound-mediated blood--brain barrier opening in vivo. *J. Cereb. Blood Flow Metab. Off. J. Int. Soc. Cereb. Blood Flow Metab.* **35**, 611–22 (2015).
63. Choi, J. J. *et al.* Noninvasive and Transient Blood-Brain Barrier Opening in the Hippocampus of Alzheimer's Double Transgenic Mice Using Focused Ultrasound. *Ultrason. Imaging* **30**, 189–200 (2008).
64. Samiotaki, G., Vlachos, F., Tung, Y. S. & Konofagou, E. E. A quantitative pressure and microbubble-size dependence study of focused ultrasound-induced blood-brain barrier opening reversibility in vivo using MRI. *Magn. Reson. Med.* **67**, 769–777 (2012).
65. Gonzalez, R. C., Woods, R. E. (Richard E. & Eddins, S. L. *Digital Image Processing Using MATLAB*. (Dorsing Kindersley, 2004).
66. Menon, V. Clustering single cells: a review of approaches on high-and low-depth single-cell RNA-seq data. *Brief. Funct. Genomics* **17**, 240–245 (2018).
67. Cembrowski, M. S. & Menon, V. Continuous Variation within Cell Types of the Nervous System. *Trends Neurosci.* **41**, 337–348 (2018).
68. Hawrylycz, M. *et al.* Canonical genetic signatures of the adult human brain. *Nat. Neurosci.* **18**, 1832–1844 (2015).
69. Sorensen, S. A. *et al.* Correlated gene expression and target specificity demonstrate excitatory projection neuron diversity. *Cereb. Cortex N. Y. N 1991* **25**, 433–449 (2015).
70. Tasic, B. *et al.* Adult mouse cortical cell taxonomy revealed by single cell transcriptomics. *Nat. Neurosci.* **19**, 335–346 (2016).
71. Baseri, B., Choi, J. J., Tung, Y.-S. & Konofagou, E. E. Multi-modality safety assessment of blood-brain barrier opening using focused ultrasound and definity microbubbles: a short-term study. *Ultrasound Med. Biol.* **36**, 1445–59 (2010).
72. Caskey, C. F., Stieger, S. M., Qin, S., Dayton, P. A. & Ferrara, K. W. Direct observations of ultrasound microbubble contrast agent interaction with the microvessel wall. *J. Acoust. Soc. Am.* **122**, 1191–1200 (2007).
73. Caskey, C. F., Kruse, D. E., Dayton, P. A., Kitano, T. K. & Ferrara, K. W. Microbubble oscillation in tubes with diameters of 12, 25, and 195 microns. *Appl. Phys. Lett.* **88**, 1–3 (2006).
74. Zheng, H. *et al.* Ultrasound-Driven Microbubble Oscillation and Translation Within Small Phantom Vessels. *Ultrasound Med. Biol.* **33**, 1978–1987 (2007).
75. Sassaroli, E. & Hynynen, K. Cavitation Threshold of Microbubbles in Gel Tunnels by Focused Ultrasound. *Ultrasound Med. Biol.* **33**, 1651–1660 (2007).

ARTICLE IN PRESS

ARTICLE IN PRESS

76. Sassaroli, E. & Hynynen, K. Resonance frequency of microbubbles in small blood vessels: A numerical study. *Phys. Med. Biol.* **50**, 5292–5305 (2005).
77. Qin, S. & Ferrara, K. W. The Natural Frequency of Nonlinear Oscillation of Ultrasound Contrast Agents in Microvessels. *Ultrasound Med. Biol.* **33**, 1140–1148 (2007).
78. Sheikov, N. *et al.* Brain arterioles show more active vesicular transport of blood-borne tracer molecules than capillaries and venules after focused ultrasound-evoked opening of the blood-brain barrier. *Ultrasound Med. Biol.* **32**, 1399–1409 (2006).
79. Shen, L., Weber, C. R. & Turner, J. R. The tight junction protein complex undergoes rapid and continuous molecular remodeling at steady state. *J. Cell Biol.* **181**, 683–95 (2008).
80. Marchiando, A. M. *et al.* Caveolin-1-dependent occludin endocytosis is required for TNF-induced tight junction regulation in vivo. *J. Cell Biol.* **189**, 111–26 (2010).
81. Beutel, O., Maraspini, R., Pombo-García, K., Martin-Lemaitre, C. & Honigmann, A. Phase Separation of Zonula Occludens Proteins Drives Formation of Tight Junctions. *Cell* **179**, 923-936.e11 (2019).
82. Hynynen, K., McDannold, N., Sheikov, N. A., Jolesz, F. A. & Vykhodtseva, N. Local and reversible blood–brain barrier disruption by noninvasive focused ultrasound at frequencies suitable for trans-skull sonications. *NeuroImage* **24**, 12–20 (2005).
83. Deng, J. *et al.* The Role of Caveolin-1 in Blood–Brain Barrier Disruption Induced by Focused Ultrasound Combined with Microbubbles. *J. Mol. Neurosci.* **46**, 677–687 (2012).
84. Pandit, R. *et al.* Role for caveolin-mediated transcytosis in facilitating transport of large cargoes into the brain via ultrasound. *J. Controlled Release* **327**, 667–675 (2020).
85. Jordão, J. F. *et al.* Amyloid-β plaque reduction, endogenous antibody delivery and glial activation by brain-targeted, transcranial focused ultrasound. *Exp. Neurol.* **248**, 16–29 (2013).
86. Sierra, C. *et al.* Lipid microbubbles as a vehicle for targeted drug delivery using focused ultrasound-induced blood–brain barrier opening. *J. Cereb. Blood Flow Metab.* **37**, 1236–1250 (2017).
87. Kovacs, Z. I. *et al.* Disrupting the blood-brain barrier by focused ultrasound induces sterile inflammation. *Proc. Natl. Acad. Sci. U. S. A.* **114**, E75–E84 (2017).
88. Kovacs, Z. I. *et al.* Disrupting the blood-brain barrier by focused ultrasound induces sterile inflammation. *Proc. Natl. Acad. Sci. U. S. A.* **114**, E75–E84 (2017).
89. Hilgenfeldt, S., Lohse, D. & Zomack, M. Response of bubbles to diagnostic ultrasound: A unifying theoretical approach. *Eur. Phys. J. B* **4**, 247–255 (1998).
90. Yang, F. Y., Lin, Y. S., Kang, K. H. & Chao, T. K. Reversible blood-brain barrier disruption by repeated transcranial focused ultrasound allows enhanced extravasation. *J. Controlled Release* **150**, 111–116 (2011).

ARTICLE IN PRESS

ARTICLE IN PRESS

91. Merlini, M. *et al.* Fibrinogen Induces Microglia-Mediated Spine Elimination and Cognitive Impairment in an Alzheimer's Disease Model. *Neuron* **101**, 1099-1108.e6 (2019).
92. Hatch, R. J., Leinenga, G. & Götz, J. Scanning Ultrasound (SUS) Causes No Changes to Neuronal Excitability and Prevents Age-Related Reductions in Hippocampal CA1 Dendritic Structure in Wild-Type Mice. *PLOS ONE* **11**, e0164278 (2016).
93. Olumolade, O. O., Wang, S., Samiotaki, G. & Konofagou, E. E. Longitudinal Motor and Behavioral Assessment of Blood-Brain Barrier Opening with Transcranial Focused Ultrasound. *Ultrasound Med. Biol.* **42**, 2270–82 (2016).
94. Strickland, S. Blood will out: vascular contributions to Alzheimer's disease. *J. Clin. Invest.* **128**, 556–563 (2018).
95. Schachtrup, C. *et al.* Development/Plasticity/Repair Fibrinogen Triggers Astrocyte Scar Formation by Promoting the Availability of Active TGF-after Vascular Damage. (2010) doi:10.1523/JNEUROSCI.0137-10.2010.
96. Akassoglou, K., Yu, W.-M., Akpinar, P. & Strickland, S. Fibrin Inhibits Peripheral Nerve Remyelination by Regulating Schwann Cell Differentiation. *Neuron* **33**, 861–875 (2002).
97. Weisel, J. W. Fibrinogen and fibrin. *Adv. Protein Chem.* **70**, 247–99 (2005).
98. Sofroniew, M. V. Molecular dissection of reactive astrogliosis and glial scar formation. *Trends Neurosci.* **32**, 638–647 (2009).
99. McMahon, D., Lassus, A., Gaud, E., Jeannot, V. & Hynynen, K. Microbubble formulation influences inflammatory response to focused ultrasound exposure in the brain. *Sci. Rep.* **10**, 1–15 (2020).
100. Shinozaki, Y. *et al.* Transformation of Astrocytes to a Neuroprotective Phenotype by Microglia via P2Y1 Receptor Downregulation. *Cell Rep.* **19**, 1151–1164 (2017).
101. McMahon, D., Bendayan, R. & Hynynen, K. Acute effects of focused ultrasound-induced increases in blood-brain barrier permeability on rat microvascular transcriptome. *Sci. Rep.* **7**, 45657 (2017).
102. Kovacs, Z. I. *et al.* MRI and histological evaluation of pulsed focused ultrasound and microbubbles treatment effects in the brain. *Theranostics* **8**, 4837–4855 (2018).
103. Bush, T. G. *et al.* Leukocyte Infiltration, Neuronal Degeneration, and Neurite Outgrowth after Ablation of Scar-Forming, Reactive Astrocytes in Adult Transgenic Mice. *Neuron* **23**, 297–308 (1999).
104. Anderson, M. A. *et al.* Astrocyte scar formation aids central nervous system axon regeneration. *Nature* **532**, 195–200 (2016).
105. Silver, J. & Miller, J. H. Regeneration beyond the glial scar. *Nat. Rev. Neurosci.* **5**, 146–156 (2004).
106. Liddelow, S. A. *et al.* Neurotoxic reactive astrocytes are induced by activated microglia. *Nature* **541**, 481–487 (2017).

ARTICLE IN PRESS

ARTICLE IN PRESS

107. Stevens, B. *et al.* The Classical Complement Cascade Mediates CNS Synapse Elimination. *Cell* **131**, 1164–1178 (2007).

108. Hong, S. *et al.* Complement and microglia mediate early synapse loss in Alzheimer mouse models. *Science* **352**, 712–716 (2016).

109. Scarcelli, T. *et al.* Stimulation of hippocampal neurogenesis by transcranial focused ultrasound and microbubbles in adult mice. *Brain Stimulat.* **7**, 304–307 (2014).

110. Mooney, S. J. *et al.* Focused ultrasound-induced neurogenesis requires an increase in blood-brain barrier permeability. *PLoS ONE* **11**, (2016).

111. Mooney, S. J., Nobrega, J. N., Levitt, A. J. & Hynynen, K. Antidepressant effects of focused ultrasound induced blood-brain-barrier opening. *Behav. Brain Res.* **342**, 57–61 (2018).

112. Burgess, A. *et al.* Alzheimer Disease in a Mouse Model: MR Imaging–guided Focused Ultrasound Targeted to the Hippocampus Opens the Blood-Brain Barrier and Improves Pathologic Abnormalities and Behavior. *Radiology* **273**, 736–745 (2014).

113. Batts, A. J. *et al.* Using a novel rapid alternating steering angles pulse sequence to evaluate the impact of theranostic ultrasound-mediated ultra-short pulse length on blood-brain barrier opening volume and closure, cavitation mapping, drug delivery feasibility, and safety. *Theranostics* **13**, 1180–1197 (2023).

114. Pouliopoulos, A. N. *et al.* Safety evaluation of a clinical focused ultrasound system for neuronavigation guided blood-brain barrier opening in non-human primates. *Sci. Rep.* **11**, 15043 (2021).

115. Han, M., Seo, H., Choi, H., Lee, E.-H. & Park, J. Localized Modification of Water Molecule Transport After Focused Ultrasound-Induced Blood-Brain Barrier Disruption in Rat Brain. *Front. Neurosci.* **15**, 685977 (2021).

116. Mathew, A. S., Gorick, C. M. & Price, R. J. Single-cell mapping of focused ultrasound-transfected brain. *Gene Ther.* **30**, 255–263 (2023).

117. O'Reilly, M. A., Huang, Y. & Hynynen, K. The impact of standing wave effects on transcranial focused ultrasound disruption of the blood-brain barrier in a rat model. *Phys. Med. Biol.* **55**, 5251–5267 (2010).

118. Tang, S. C. & Clement, G. T. Acoustic standing wave suppression using randomized phase-shift-keying excitations. *J. Acoust. Soc. Am.* **126**, 1667 (2009).

119. Connor, C. W. & Hynynen, K. Patterns of thermal deposition in the skull during transcranial focused ultrasound surgery. *IEEE Trans. Biomed. Eng.* **51**, 1693–1706 (2004).

ARTICLE IN PRESS

ARTICLE IN PRESS

120. Asquier, N. *et al.* Blood-brain barrier disruption in humans using an implantable ultrasound device: quantification with MR images and correlation with local acoustic pressure. *J. Neurosurg.* 1–9 (2019) doi:10.3171/2018.9.JNS182001.

121. Prakash, R., & Carmichael, S. T. Blood-brain barrier breakdown and neovascularization processes after stroke and traumatic brain injury. *Current opinion in neurology*. **28**, 556–564 (2015).

122. Protzmann, J., Jung, F., Jakobsson, L., & Fredriksson, L. Analysis of ischemic stroke-mediated effects on blood-brain barrier properties along the arteriovenous axis assessed by intravital two-photon imaging. *Fluids and barriers of the CNS*. **21,** 35 (2024).

Acknowledgements

We thank Shutao Wang, Camilo Acosta, and Daniella Jimenez for their supporting role in this work. T.K., R.L.N., R.J. and E.E.K. are supported by the National Institute on Aging of the National Institutes of Health under Award Number R01AG038961. D.A. is supported by the NIH (R01EY033994; R61/33 HL159949; RF1 AG078352, R21NS130265) and by an unrestricted gift to the Division of Cerebrovascular Diseases and Stroke in the Department of Neurology, CUIMC. The content is solely the responsibility of the authors and does not necessarily represent the official views of the National Institutes of Health.

Author contributions

T. K., D.A. and E. E. K. conceptualized the project, R.L.N., T. K., M. E. K., C. S. C, S.S., Y. N. and R.J. performed the experiments and analyzed the data, D. A. provided the transgenic mice, D.A. and E.E.K. provided guidance for the analysis of the data & T. K., R.L.N. D.A. and E.E.K wrote and edited the manuscript.

Ethics Declarations

All experimental procedures involving animals were approved by the Columbia University Institutional Animal Care and Use Committee (IACUC) and in accordance to the Office of Laboratory Animal Welfare and the Association for Assessment and Accreditation of Laboratory Care regulations.

Conflicts of interest

Some of the work presented is supported by patents optioned to Delsona Therapeutics, Inc. where EEK serves as a co-founder and scientific advisor. The remaining authors declare no competing interests.

ARTICLE IN PRESS

ARTICLE IN PRESS

Additional Information

The Supplementary Information associated with this manuscript contains 10 Extended Data figures and legends, 8 supplementary data related to the single-cell RNA sequencing data and 4 supplementary movies.

Figure Legends

Figure 1. FUS with microbubble induces transient BBB opening only at safe pressures.

(**A**) Schematic diagram of the experimental paradigm. (**B**) Quantification of the stable cavitation dose (SCD) for harmonics (SCDh) and ultra-harmonics (SCDu), and inertial cavitation dose (ICD) for 450 kPa (N=4 mice) and 750 kPa (N=5 mice). Signals were collected from a passive cavitation detector (PCD) during a 120 second sonication interval. (**C-D**) Axial and coronal evaluation of BBB opening at 1 and 72 hours post-FUS with contrast-enhanced T1-weighted MRI in the caudate / putamen region for 450 kPa (**C**) and 750 kPa (**D**). The BBB becomes permeable at both pressures after 1 hour; however, the BBB is permeable only at 750 kPa after 72 hours. (**E**) Quantification of the BBB leakage volume after gadolinium injection administered 1 and 72 hours post-FUS (N=4 mice/group; *p<0.05 and ****p<0.0001; two-way ANOVA with Sidak's multiple comparison test). (**F, G**) *eGFP-Claudin5*$^{+/-}$ mice were injected with biocytin-TMR (870 Da) after FUS to determine BBB permeability. Brain sections show biocytin-TMR leakage in the ipsilateral caudate/putamen region 1 hour after FUS at 450 and 750 kPa. Scale bars = 200 µm (**H**) Quantification of biocytin-TMR fluorescence intensity normalized to optical density between ipsilateral and contralateral matched regions of interest (ROIs) at 450 and 750 kPa 1 hour after FUS (N=4 mice/group; **p<0.01 and ****p<0.0001; two-way ANOVA with Sidak's multiple comparison test; a.u., arbitrary unit). (**I**) Quantification of biocytin-TMR leakage area at 450 kPa and 750 kPa one hour after FUS (N=4 mice/ group; *p<0.05; Student's t-test). (**J-K**) Brain sections show biocytin-TMR leakage in the caudate/putamen region 72 hours after FUS at 450 (N=4) and 750 kPa (N=5). (**L**) Quantification of biocytin-TMR fluorescence intensity normalized to optical density between ipsilateral and contralateral matched ROIs at 450 (N=4) and 750 kPa (N=5) 72 hours after FUS (*p<0.05; two-way ANOVA with Sidak's multiple comparison test; a.u., arbitrary unit). (**M**) Quantification of biocytin-TMR leakage area at 450 (N=4) and 750 kPa (N=5) 72 hours after FUS. Student's t-test was used for statistical comparisons (p = 0.1106). Data are presented as mean± standard deviation. Arrowheads denote the area of biocytin extravasation. See also **Extended Data Figure 1**.

Figure 2. Persistent abnormal tight junctions in capillaries correlate with continuous BBB opening at higher pressures.

ARTICLE IN PRESS

(**A**) Quantification of the average number of leaky small (<10 µm) and large (>10µm) vessels per brain section at 450 and 750 kPa 1 hour after FUS (N=4 mice / group; **p<0.01; # p = 0.0569; Student's t-test). (**B**) Quantification of the fraction of small and large leaky vessels at 450 kPa and 750 kPa one hour after FUS. The fraction of leaky vessels is higher for larger caliber vessels at high pressure (N=4 mice/group; *p<0.05; two-way ANOVA with Sidak's multiple comparison test). (**C**) Quantification of the average number of leaky small (<10 µm) and large (>10µm) vessels per brain section at 72 hours after FUS at 450 kPa and 750 kPa (N=4-5 mice / group; **p<0.01, ## p = 0.0682; Student's t-test). (**D**) Quantification of the fraction of small and large leaky vessels at 750 kPa compared to 450 kPa at 72 hours after FUS (N=4-5 mice/group; ***p<0.001, **p<0.01 two-way ANOVA with Sidak's multiple comparison test). (**E-H"; K-N"**) Maximum intensity projection images of 25µm-thick caudate putamen sections from *eGFP-Claudin5*$^{+/-}$ mice sonicated at 450 kPa (**E-F"**) and 750 kPa (**G-H"**). The images show capillaries in the ipsilateral and contralateral caudate / putamen regions at 1 (**E-H"**) and 72 (**K-N"**) hours after FUS. eGFP (green) labels TJs in capillaries. Biocytin-TMR leakage (red) is found in the ipsilateral parenchyma. GLUT-1 (white) labels endothelial cells. The absence of TJ strand in vessels is indicated by white arrowheads. (**I**) Quantification of the TJ gap size in contralateral and ipsilateral caudate / putamen at 450 kPa and 750 kPa at 1 hour post-FUS. (J-K) Quantification of fraction of TJ strands with gaps > 2.5 µm at 450 kPa and 750 kPa at 1 and 72 hours post-FUS. The fraction of TJ strands with gaps greater than 2.5 µm is significantly different in the ipsilateral compared to the contralateral hemisphere at 750 kPa (N=5-7 mice / group; ∗p < 0.05; **p<0.01, ****p<0.0001, one-way ANOVA with Sidak's multiple comparison test). All data are presented as mean± standard deviation. Scale bars = 20 µm. See also **Extended Data Figures 2-7**.

Figure 3. Single-cell RNA-sequencing of brain endothelial cells after FUS-BBBO and identification of vessel subtypes. (**A**) Experimental workflow for single-cell RNA-sequencing of BECs after FUS (created with BioRender.com). (**B-D**) Uniform manifold approximation and projection (UMAP) of BECs integrated and color coded by Seurat cluster (numbers refer to each color coded cluster), treatment group, and sequencing batch, respectively. (**E**) Clusters of arterial, capillary and venous cells in the UMPA plot identified by expression of canonical markers Bmx, Msfd2a and Nr2f2, respectively. (**F**) Dotted plot of canonical markers used to identify arterial, capillary and venous BECs. Numbers annotating the arterial, capillary, and venous endothelial populations correspond to the cluster IDs shown in **Figure 3B**. The size of the dot indicates the number of cells and the color the intensity of expression. (**G**) Dotted bar plot showing the percentage of arterial, capillary, and venous BECs for each treatment group. See also **Extended Data Figure 8** and **Supplementary Data 1-4**.

ARTICLE IN PRESS

Figure 4. Gene ontology analysis of differentially expressed genes in capillary BECs for each condition from single cell RNA sequencing. (**A**) Gene ontology terms upregulated in FUS (450 + 750 kPa) capillary BECs compared to untreated controls 1 hour post-FUS. (**B**) Gene ontology terms upregulated in capillary BECs exposed to 450 kPa (green) and 750 kPa (blue) compared to untreated controls, 72 hours post-FUS-BBBO. (**C**) Gene ontology terms upregulated in capillary BECs exposed to 750 kPa compared to 450 kPa cells 72 hours post-FUS-BBBO. In all bar plots the bar represents the -Log_2(FDR) (top axis), and the dot represents the number of significantly annotated genes (bottom axis). (**D**) Dot plot showing relative expression of key genes annotated to the upregulated gene ontology terms for each treatment group and untreated controls. The size of the dot indicates the number of cells and the color the intensity of expression. (**E-G**) Dot plot showing relative expression of key adherens and tight junction genes in arterial, capillary and venous BECs for each treatment group and untreated controls. The size of the dot indicates the number of cells and the color the intensity of expression. See also **Extended Data Figure 9** and **Supplementary Data 5-7**.

Figure 5. Gene set enrichment analysis (GSEA) results for capillary BECs after FUS-BBBO. (**A**) GSEA pathways up and downregulated in capillary BECs for the indicated comparisons (P value cutoff < 0.3). Bars represent the -Log_2(FDR) values (left y-axis), and dots represent the number of significant genes annotated to each pathway (right y-axis). Comparison label convention is "Measured vs. Reference". For example, "FUS vs Control" represents changes observed in FUS groups using the Control group as reference. (**B-D**) Violin plots showing the expression of representative genes for TGF-β Signaling, Notch Signaling, and Canonical Wnt Signaling. Statistical significance was measured between each group and the Control using pairwise Wilcoxon rank sum tests to determine the adjusted p-value. The two pressures (450 + 750 kPa) were pooled for 1 hour post-FUS-BBBO for this analysis. Significance values are indicated as follows: *$p \leq 0.05$, **$p \leq 0.01$, ****$p \leq 0.001$.

Figure 6. BECs exposed to higher pressure after FUS-BBBO exhibit a sustained increase in Egfl7 mRNA expression.

(**A**) Violin plots showing expression of *Egfl7* mRNA across each of the treatment groups. Mean expression level is indicated by the bar. Statistically significant differences between each group and untreated controls are determined by Wilcoxon rank sum test, **** $p \leq 0.0001$. BECs exposed to 450 kPa (**B**) exhibit modest increase in *Egfl7* mRNA expression compared to the untreated contralateral hemisphere (**C**). BECs exposed to 750 kPa (**D**) exhibit markedly increase in *Egfl7* mRNA levels relative to the untreated contralateral hemisphere (**E**). White arrowheads indicate Glut-1^+ vessels with positive *Egfl7* mRNA expression. See also **Extended Data Figure 10**.

ARTICLE IN PRESS

Editor's Summary:
Focused ultrasound can transiently open the blood–brain barrier for drug delivery, but the cellular responses of brain endothelial cells remain unclear. Rebecca Lynn Noel and colleagues report how low or high ultrasound pressures differently reorganize tight junction proteins, defining conditions for safe and reversible barrier opening.

Peer review information:
Communications Engineering thanks Wenlu Li and the other, anonymous, reviewer(s) for their contribution to the peer review of this work. Primary Handling Editors: [Liangfei Tian] and [Philip Coatsworth]. A peer review file is available.

ARTICLE IN PRESS

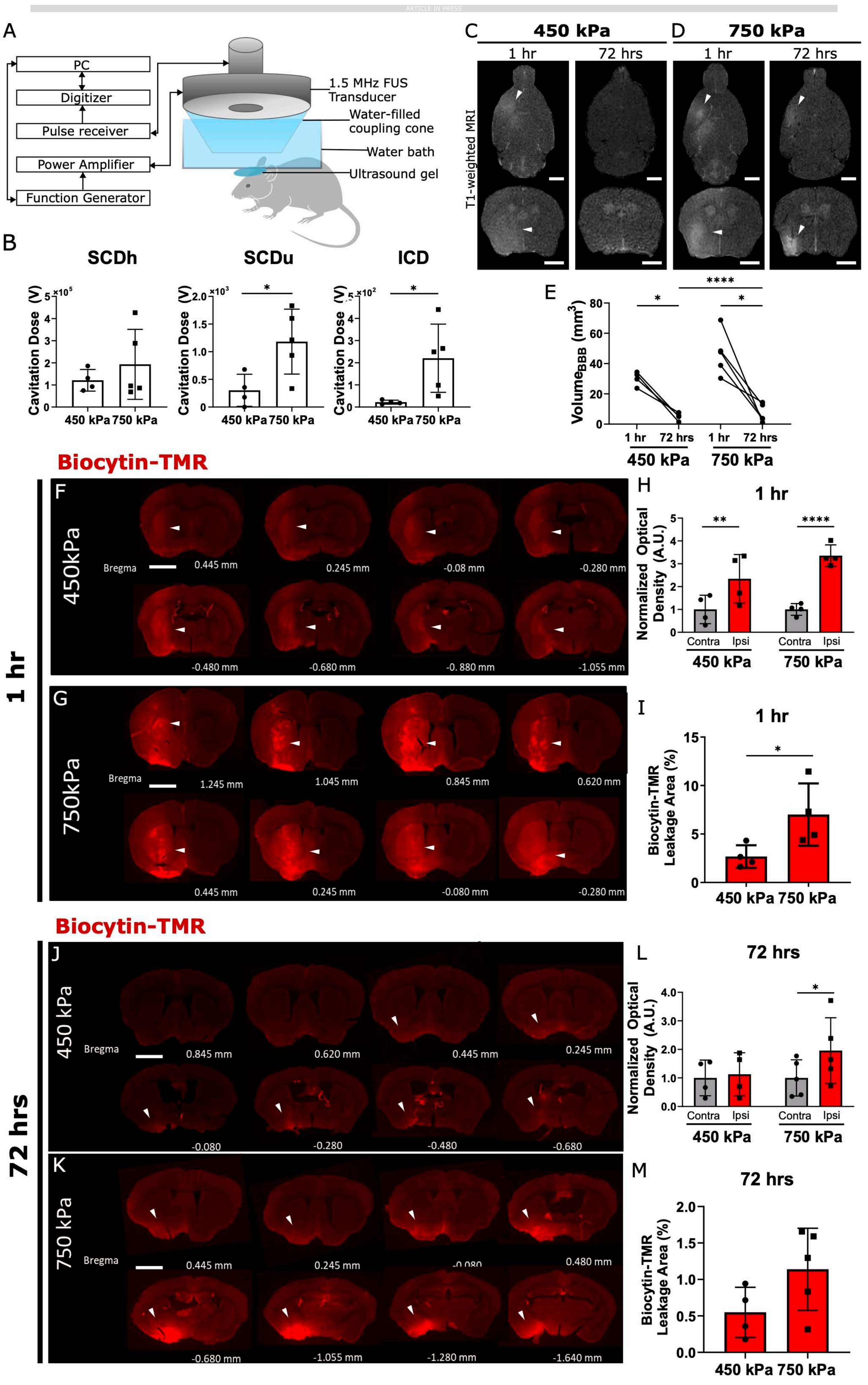
A
PC
Digitizer
Pulse receiver
Power Amplifier
Function Generator
1.5 MHz FUS Transducer
Water-filled coupling cone
Water bath
Ultrasound gel
B
SCDh
SCDu
ICD
Cavitation Dose (V)
450 kPa
750 kPa
C
450 kPa
D
750 kPa
1 hr
72 hrs
T1-weighted MRI
E
Volume$_{BBB}$ (mm^3)
Biocytin-TMR
F
450kPa
Bregma
0.445 mm
0.245 mm
-0.08 mm
-0.280 mm
-0.480 mm
-0.680 mm
-0. 880 mm
-1.055 mm
G
750kPa
1.245 mm
1.045 mm
0.845 mm
0.620 mm
0.445 mm
0.245 mm
-0.080 mm
-0.280 mm
H
Normalized Optical Density (A.U.)
Contra
Ipsi
I
Biocytin-TMR Leakage Area (%)
J
K
L
M
-0.080
-0.280
-0.480
-0.680
0.845 mm
0.620 mm
0.445 mm
0.245 mm
0.480 mm
-1.055 mm
-1.280 mm
-1.640 mm

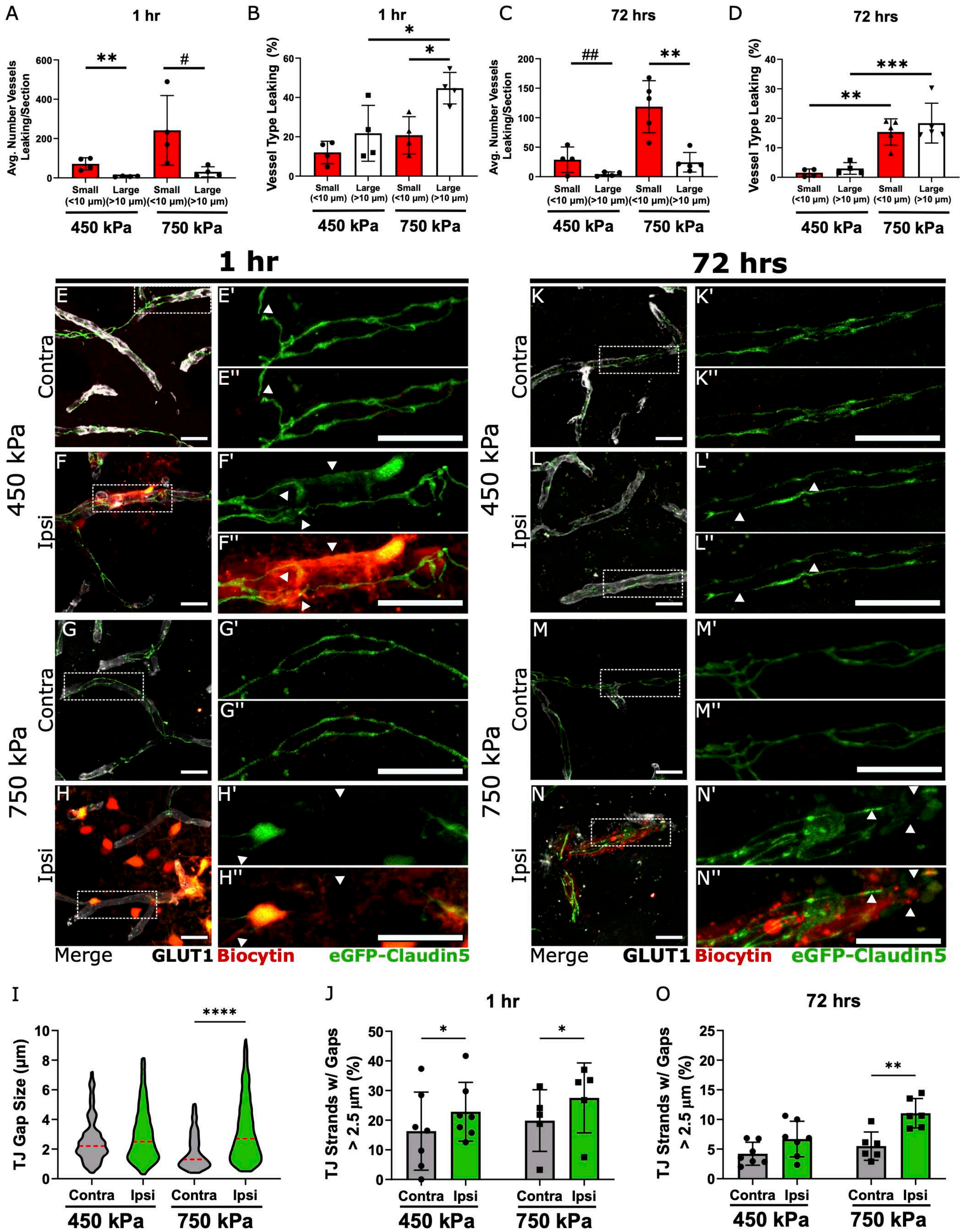
A
1 hr
Avg. Number Vessels Leaking/Section
Small (<10 µm)
Large (>10 µm)
450 kPa
750 kPa
B
1 hr
Vessel Type Leaking (%)
C
72 hrs
D
72 hrs
1 hr
72 hrs
450 kPa
750 kPa
Contra
Ipsi
Merge
GLUT1
Biocytin
eGFP-Claudin5
I
TJ Gap Size (µm)
Contra
Ipsi
J
TJ Strands w/ Gaps > 2.5 µm (%)
O

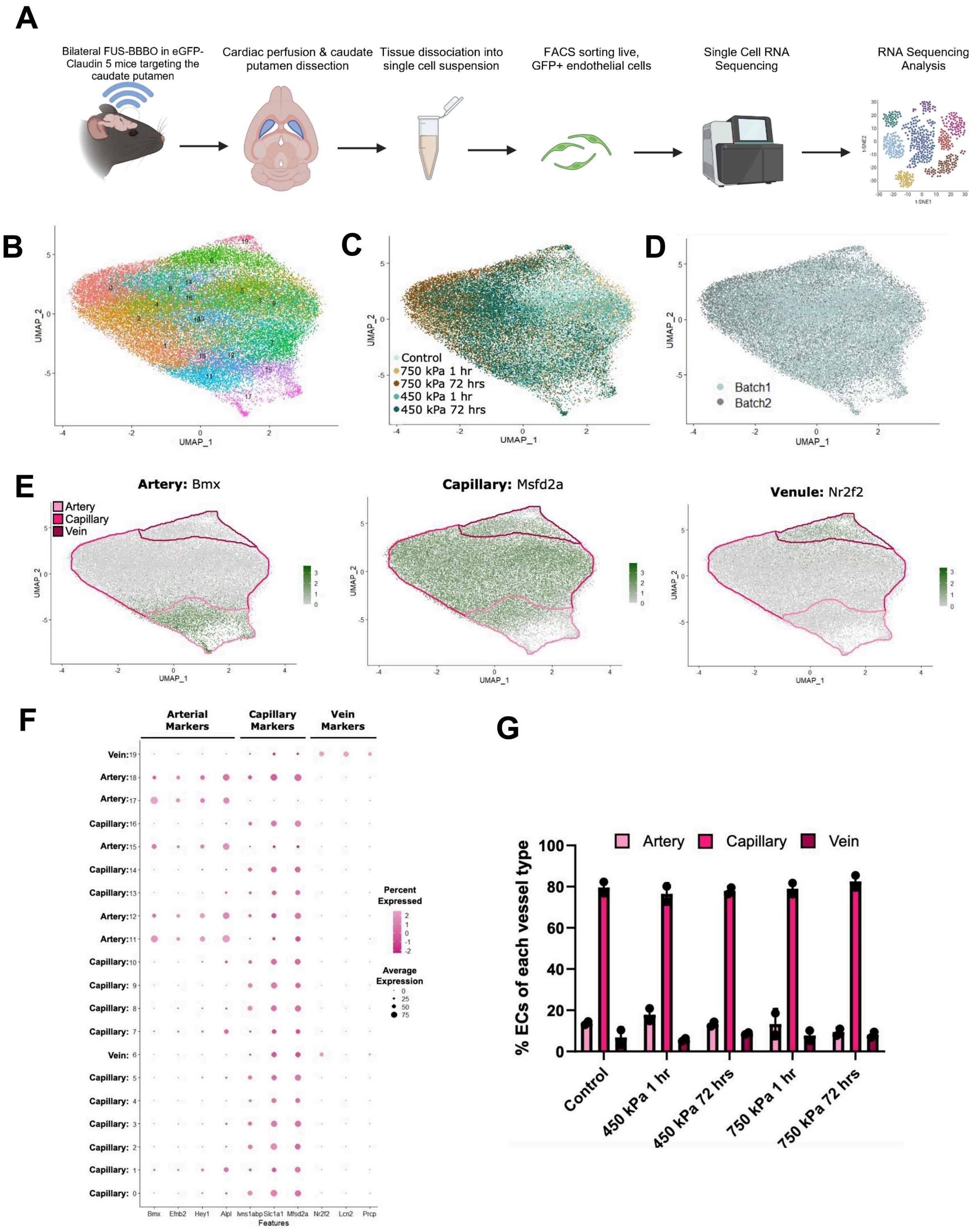
A
Bilateral FUS-BBBO in eGFP-Claudin 5 mice targeting the caudate putamen
Cardiac perfusion & caudate putamen dissection
Tissue dissociation into single cell suspension
FACS sorting live, GFP+ endothelial cells
Single Cell RNA Sequencing
RNA Sequencing Analysis
t-SNE1
t-SNE2
B
UMAP_1
UMAP_2
C
Control
750 kPa 1 hr
750 kPa 72 hrs
450 kPa 1 hr
450 kPa 72 hrs
D
Batch1
Batch2
E
Artery: Bmx
Capillary: Msfd2a
Venule: Nr2f2
Artery
Capillary
Vein
F
Arterial Markers
Capillary Markers
Vein Markers
Percent Expressed
Average Expression
Bmx
Efnb2
Hey1
Alpl
Ivns1abp
Slc1a1
Mfsd2a
Nr2f2
Lcn2
Prcp
Features
G
Artery
Capillary
Vein
% ECs of each vessel type
Control
450 kPa 1 hr
450 kPa 72 hrs
750 kPa 1 hr
750 kPa 72 hrs

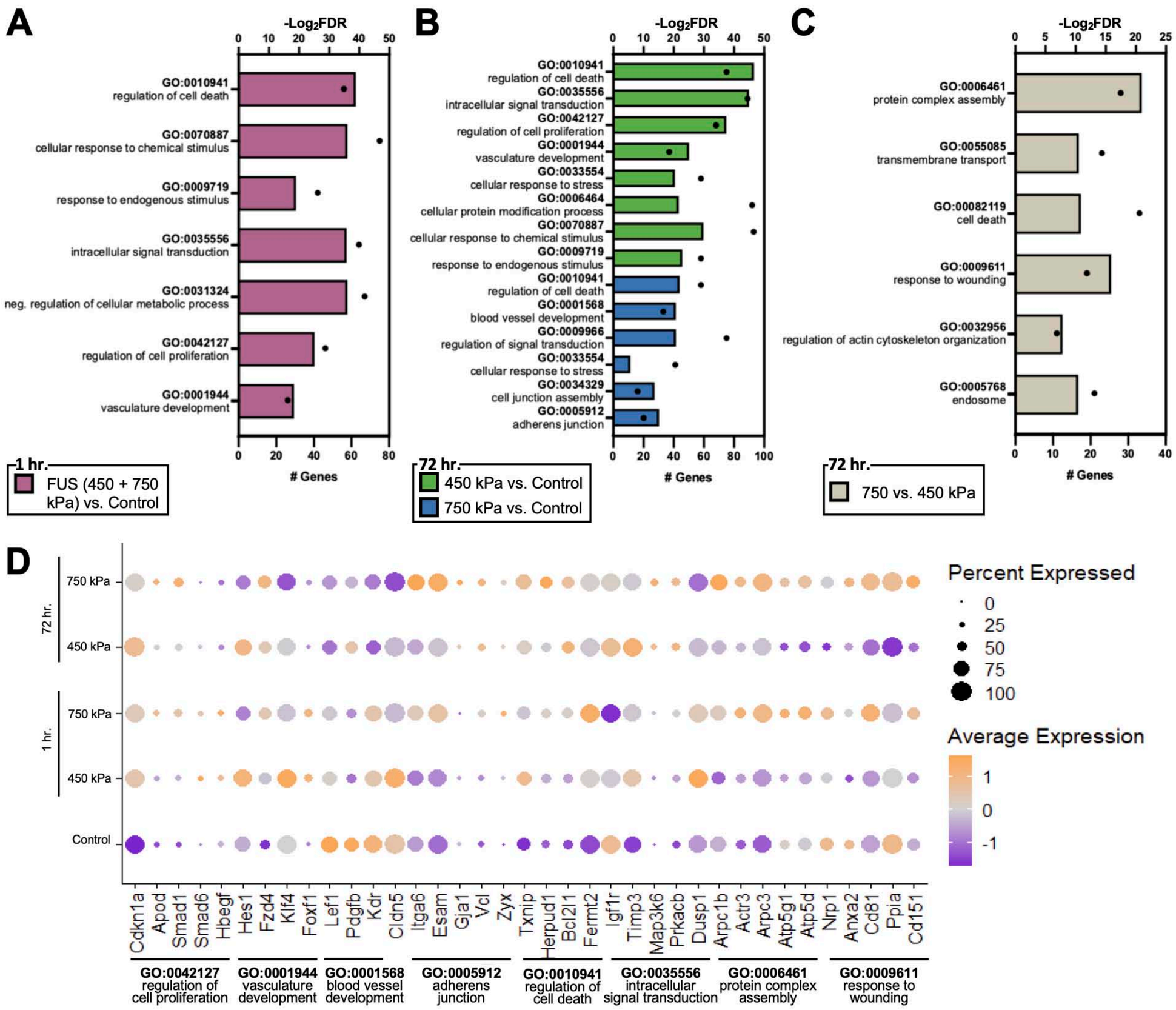
A
-Log2FDR
GO:0010941 regulation of cell death
GO:0070887 cellular response to chemical stimulus
GO:0009719 response to endogenous stimulus
GO:0035556 intracellular signal transduction
GO:0031324 neg. regulation of cellular metabolic process
GO:0042127 regulation of cell proliferation
GO:0001944 vasculature development
Genes
1 hr.
FUS (450 + 750 kPa) vs. Control
B
GO:0010941 regulation of cell death
GO:0035556 intracellular signal transduction
GO:0042127 regulation of cell proliferation
GO:0001944 vasculature development
GO:0033554 cellular response to stress
GO:0006464 cellular protein modification process
GO:0070887 cellular response to chemical stimulus
GO:0009719 response to endogenous stimulus
GO:0010941 regulation of cell death
GO:0001568 blood vessel development
GO:0009966 regulation of signal transduction
GO:0033554 cellular response to stress
GO:0034329 cell junction assembly
GO:0005912 adherens junction
72 hr.
450 kPa vs. Control
750 kPa vs. Control
C
GO:0006461 protein complex assembly
GO:0055085 transmembrane transport
GO:00082119 cell death
GO:0009611 response to wounding
GO:0032956 regulation of actin cytoskeleton organization
GO:0005768 endosome
72 hr.
750 vs. 450 kPa
D
750 kPa
450 kPa
Control
Percent Expressed
Average Expression
Cdkn1a Apod Smad1 Smad6 Hbegf Hes1 Fzd4 Klf4 Foxf1 Lef1 Pdgfb Kdr Cldn5 Itga6 Esam Gja1 Vcl Zyx Txnip Herpud1 Bcl2l1 Fermt2 Igf1r Timp3 Map3k6 Prkacb Dusp1 Arpc1b Actr3 Arpc3 Atp5g1 Atp5d Nrp1 Anxa2 Cd81 Ppia Cd151
GO:0042127 regulation of cell proliferation
GO:0001944 vasculature development
GO:0001568 blood vessel development
GO:0005912 adherens junction
GO:0010941 regulation of cell death
GO:0035556 intracellular signal transduction
GO:0006461 protein complex assembly
GO:0009611 response to wounding

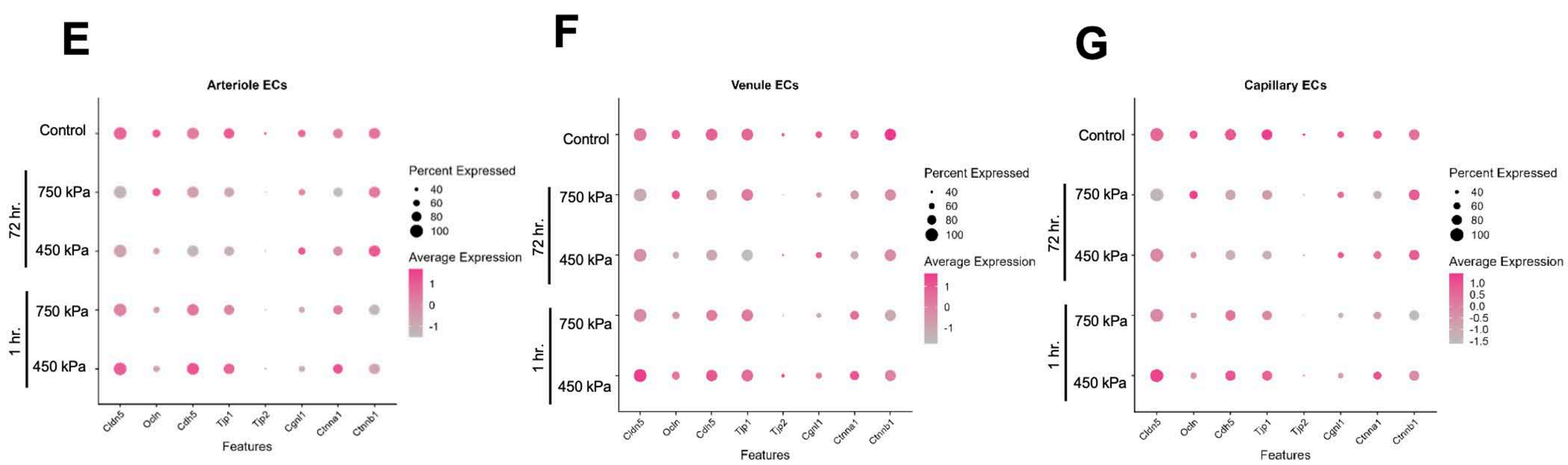
E
Arteriole ECs
Control
750 kPa
450 kPa
Percent Expressed
Average Expression
Cldn5 Ocln Cdh5 Tjp1 Tjp2 Cgnl1 Ctnna1 Ctnnb1
Features
F
Venule ECs
G
Capillary ECs

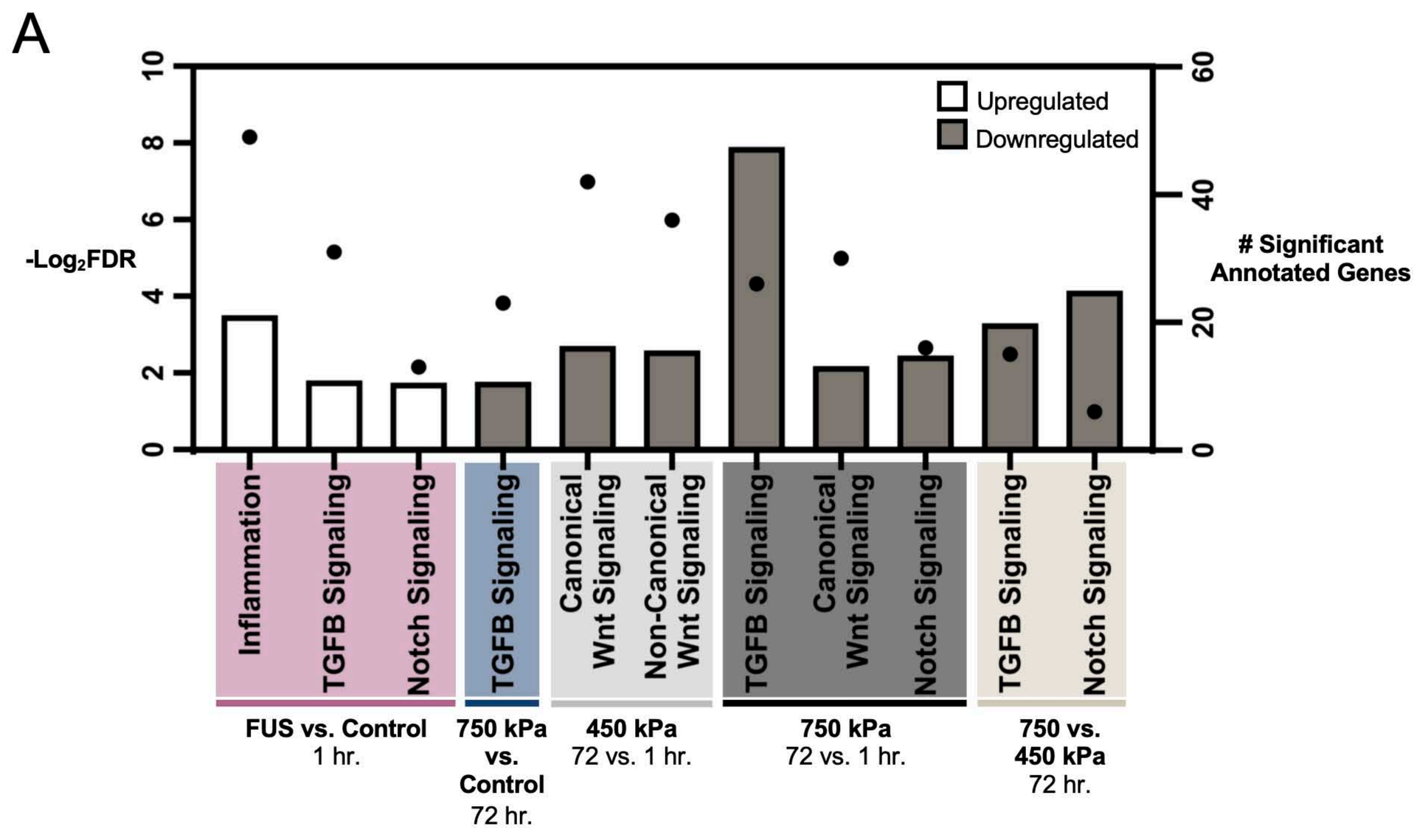
A
Upregulated
Downregulated
-Log2FDR
Significant Annotated Genes
Inflammation
TGFB Signaling
Notch Signaling
TGFB Signaling
Canonical Wnt Signaling
Non-Canonical Wnt Signaling
TGFB Signaling
Canonical Wnt Signaling
Notch Signaling
TGFB Signaling
Notch Signaling
FUS vs. Control 1 hr.
750 kPa vs. Control 72 hr.
450 kPa 72 vs. 1 hr.
750 kPa 72 vs. 1 hr.
750 vs. 450 kPa 72 hr.

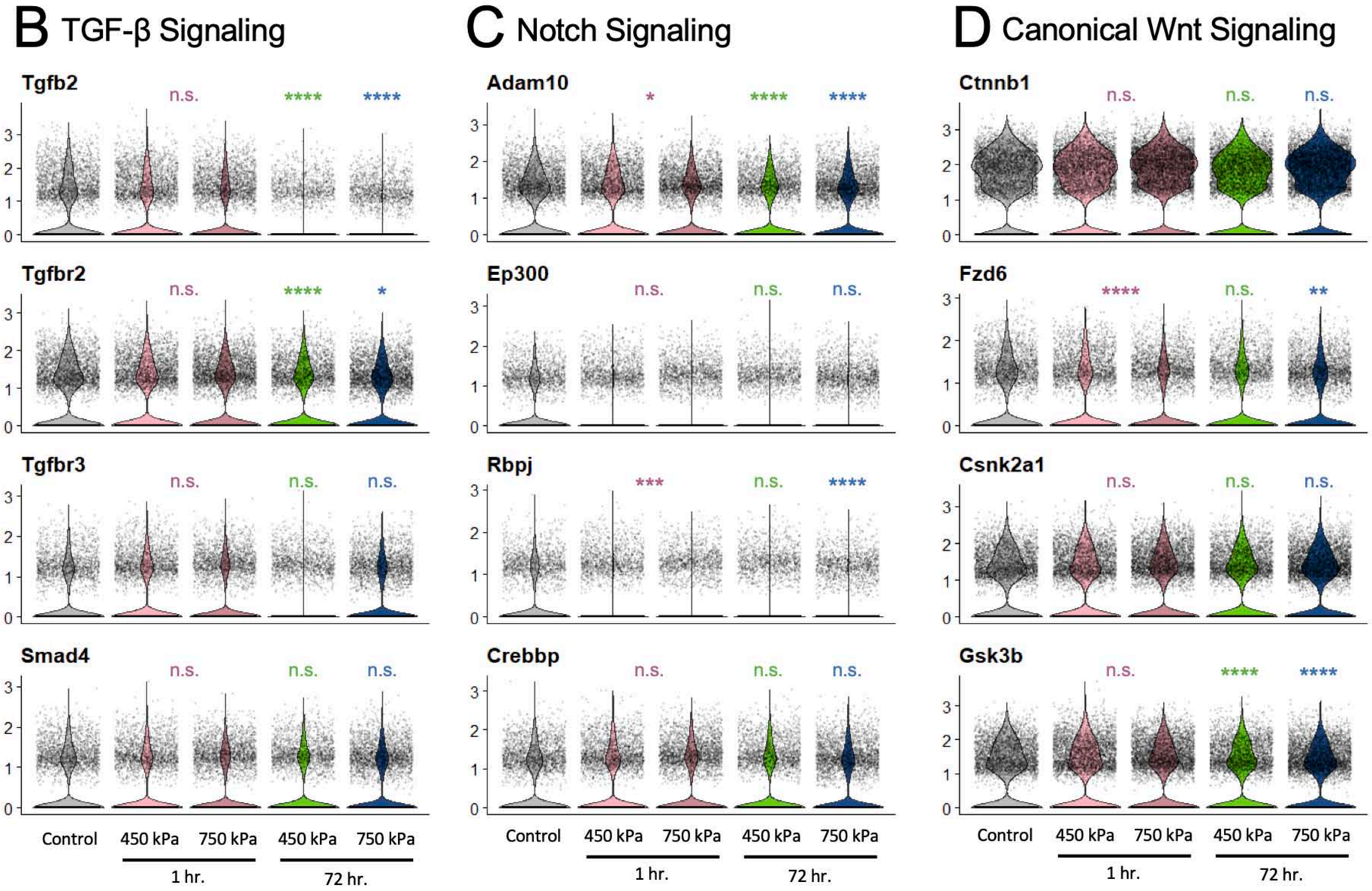
B TGF-β Signaling
C Notch Signaling
D Canonical Wnt Signaling
Tgfb2
Tgfbr2
Tgfbr3
Smad4
Adam10
Ep300
Rbpj
Crebbp
Ctnnb1
Fzd6
Csnk2a1
Gsk3b
Control
450 kPa
750 kPa
1 hr.
72 hr.

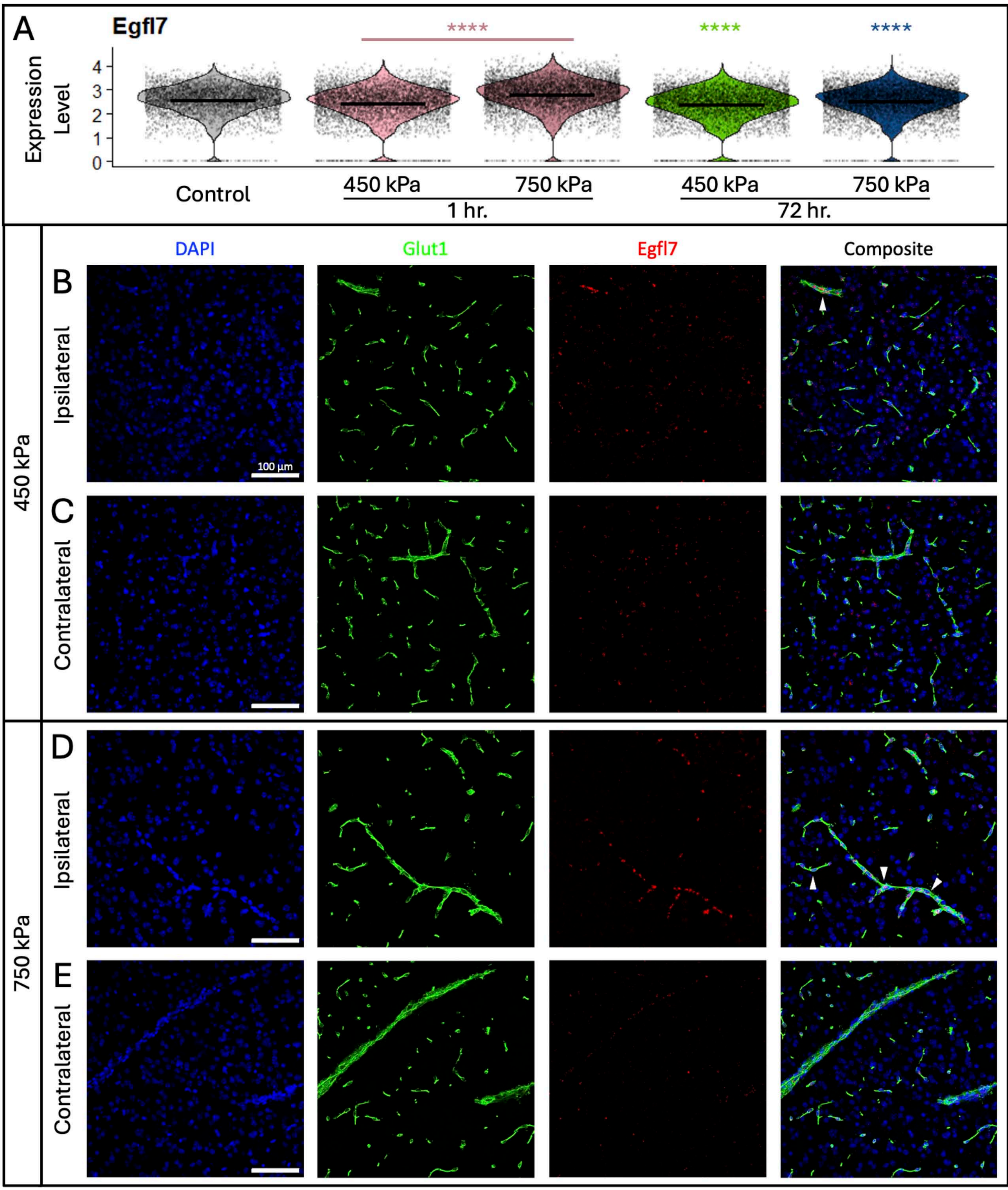
A
Egfl7
****
****
****
Expression Level
4
3
2
1
0
Control
450 kPa
750 kPa
1 hr.
450 kPa
750 kPa
72 hr.
DAPI
Glut1
Egfl7
Composite
B
Ipsilateral
100 µm
C
Contralateral
450 kPa
D
Ipsilateral
E
Contralateral
750 kPa